DISTRIBUTION OF THE HURRICANE HARVEY DEPOSIT ON THE BRAZOS SUBAQUEOUS DELTA

A Thesis

by

CHRISTENA ELIZABETH HOELSCHER

Submitted to the Graduate and Professional School of
Texas A&M University
in partial fulfillment of the requirements for the degree of

MASTER OF SCIENCE

Chair of Committee,	Timothy Dellapenna
Committee Members,	Niall Slowey
	Jens Figlus
Head of Department,	Shari Yvon-Lewis

December 2021

Major Subject: Oceanography

ABSTRACT

Hurricane Harvey (Harvey) brought over 100 cm of rain to the lower drainage basin of the Brazos River, resulting in the highest discharge event in the river's recorded history. The purpose of this project is to delineate the Brazos subaqueous delta flood deposit from Harvey, track its migration pattern, and determine the significance extratropical storm activity has on the remobilization of the deposit. On the September 2017 research cruise, during the waning phase of the flood, 15 box cores were collected across the nearshore subaqueous Brazos River Delta. Follow-up cruises occurred in October 2017 and July 2018 to help track the migration of the flood deposit. After observing multiple characteristics of the cores, results show that the Harvey flood deposit had an average thickness of 10.5 cm, with the thickest deposit reaching 24.8 cm. A total sediment yield for Hurricane Harvey of 24.5×10^6 metric tons was delivered to the GOM by the Brazos River, where 80% of the sediment was captured by the delta. Subsequent mapping of the flood deposit indicates that after initial deposition, the flood deposit has migrated offshore and to the west of its original deposition site, due to a combination of substantial extratropical storm activity and strong sea breezes between September 2017 and July 2018. Along with the sediment, organic matter, particle-bound contaminants, and nutrients are also stored in the storm deposit. This deposit will potentially be available for re-mobilization due to active shelf processes, which can introduce the nutrients and contaminants to the water column.

ACKNOWLEDGEMENTS

I would like to thank my committee chair, Dr. Dellapenna, and my committee members Dr. Slowey and Dr. Figlus for their time, guidance, and support through out this research.

Thanks also goes to my collaborators at Woods Hole University and Joe Carlin for their support, and my friends and colleagues for making my time at Texas A&M University a memorable one.

CONTRIBUTORS AND FUNDING SOURCES

Contributors

This work was supervised by a thesis committee consisting of Dr. Dellapenna (Advisor) of the Department of Oceanography and Dr. Niall Slowey of the Department of Oceanography and Dr. Jens Figlus of the Department of Ocean Engineering.

All work conducted for the thesis was completed by the student independently.

Funding Sources

Graduate study was supported in part by a fellowship in 2018-2019 from Texas A&M University. The work was also made possible by NSF under Grant Number 1635893. Its contents are solely the responsibility of the author and do not necessarily represent the view of NSF.

NOMENCLATURE

GOM	Gulf of Mexico
TMB	Texas Mud Blanket
HFD	Harvey Flood Deposit
EN	Extratropical Northers

TABLE OF CONTENTS

Page

LIST OF FIGURES

Page

LIST OF TABLES

Page

1. INTRODUCTION

Rivers serve as important conduits for the transfer of terrestrially derived materials, including sediments, nutrients, organic matter, and contaminants to the ocean (Wright, 1977; Coleman & Prior, 1982; Milliman & Meade, 1983; Nittrouer & Wright, 1994; Goni et al., 1997; Feng et al., 1998; Kineke et al., 2000; Geyer, et al., 2004; Kuehl et al., 2004; McKee et al., 2004; Ludwig et al., 2009; Yang et al., 2012). Most studies are conducted on larger river systems due to their higher flux of these important materials, but the less studied smaller river systems might be more significant regarding the delivery of the terrestrially derived materials than originally thought due to the abundance of small and medium river systems (Wheatcroft et al., 1997). These smaller rivers usually have a low flow rate but are highly sensitive to terrestrial activities (Wheatcroft et al., 1997). For example, inland floods caused by heavy rainfall events deliver terrestrially derived material into the river and cause an increase in river discharge and sediment loads, which can be delivered to the subaerial and subaqueous portions of a delta, as well as the proximal shelf (Wheatcroft et al., 1997; Carlin et al., 2014; McGuffin, 2018; Carlin et al., 2021). When discharge from the river exits the mouth of the river, the energy fans out and reduces due to it entering a larger area with different characteristics, such as salinity and temperature (Jones et al., 2007). This causes any deposit to form a fan.

The sediment from extreme rainfall events can be deposited onto the continental shelf or delta as flood deposits, where major flood events tend to generate deposits too thick to be completely eroded and are preserved in the stratigraphy and correlated to

specific flood events. (e.g., Carlin et al., 2021). Over time, portions of these deposits can be reworked as sediment is eroded from the upper portions and dispersed via currents or wave activity often due to extratropical storms or hurricanes along the shelf to a distal depocenter (Carlin et al., 2021). Distal depocenters, depositional locations that are located off-center of the original deposition site, are common for deltas and are important in various budget studies such as organic carbon (OC) (Carlin et al., 2021). These depocenters have been found to act as sinks for flood material, which are transported there via longshore transport (Carlin et al., 2021).

The along-shelf dispersal tends to happen through a series of sediment resuspension events (Nittrouer et al., 1994). In the case of the Gulf of Mexico, this is typically driven primarily by extratropical norther (EN) passage and tropical storms (Carlin et al., 2016; Moeller et al., 1993; Roberts et al., 1987). Throughout the Holocene, a stretch of the shelf called the Texas Mud Blanket (TMB) has been identified as a distal depocenter for both the Brazos and Colorado Rivers (Shideler, 1978; Anderson et al., 2016).

The Mississippi and Brazos Rivers are the largest sediment sources to the TMB, and though the Mississippi has a larger sediment load, the Brazos contributes more due to its proximity (Carlin et al., 2021). Although throughout much of the Holocene, the Colorado and Rio Grande Rivers have also been major contributors, for much of the past century, their contributions have been minimal (Anderson et al., 2016). Surface water impoundment and removal from the Rio Grande River has reduced its flow to the point where the flow often cannot even keep the river mouth open (Banfield and Anderson,

2004). For much of the mid to late Holocene, the Colorado River emptied into Matagorda Bay forming a bayhead delta, which reduced its input into the TMB (Wadsworth, 1966). Terrestrial and lagoonal sediment make up the deepest parts of this depo-center, but much of the sediment is sourced from the Mississippi and Brazos Rivers, forming the 45 m thick mud deposit (Weight et al., 2011; Anderson et al., 2004). Most of the sediment brought to the TMB from the Brazos are portions of flood deposits that have been eroded within a year of deposition from the Brazos Delta (Carlin et al., 2021). There it is preserved, making the TMB a distal depocenter for Brazos Flood sediment (Carlin et al., 2021).

Following large floods in 2015 and 2016, McGuffin (2018) delineated a series of flood deposits across the subaqueous Brazos Delta and tracked the associated sediment dispersal to the TMB. In this study, the thickness of the flood deposit was determined by analyzing various geochemical and sedimentary characteristics including but not limited to water content, grain size, and short-lived radioisotope age dating. By observing the change in the flood deposit thickness between four different cruises (between February and September 2016), the migration of the flood deposit was observed. McGuffin (2018) found that the upper 20 cm of the TMB was sourced from remobilized Brazos Sediment,

indicating rapid transport of sediment to the TMB.

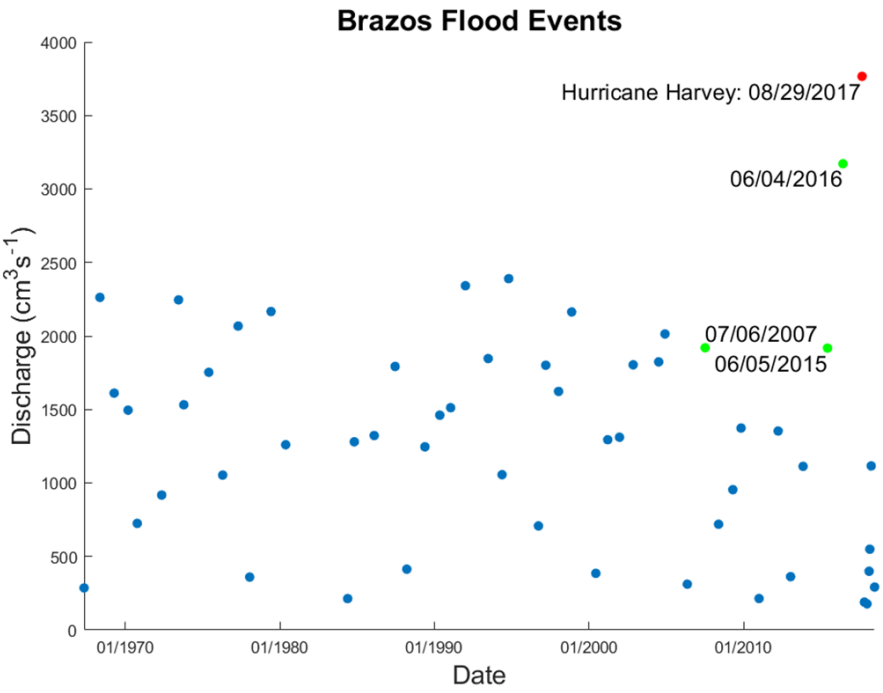

Figure 1 Historical Brazos River Peak Discharge. The last three peak discharges are noted in the figure. Note, the last two peak discharge events, 08/29/2017 and 06/04/2016, were each record discharge events. The TAMUG Coastal Geology Lab sampled the noted event

The associated flood deposit was found to be sourced from the second-largest recorded discharge event of the Brazos River (McGuffin, 2018), which, on June 4, 2016, had a maximum discharge of 3,172 m^3s^{-1}, compared to the basin average of 36.8 m^3s^{-1}, (Fig. 1) following a series of flood events that started earlier that spring (McGuffin, 2018; USGS). These floods, including the Tax Day Flood (April 16-17, 2016), were a direct result of one of the strongest El Niño events recorded (Fraticelli, 2006; McGuffin, 2018).

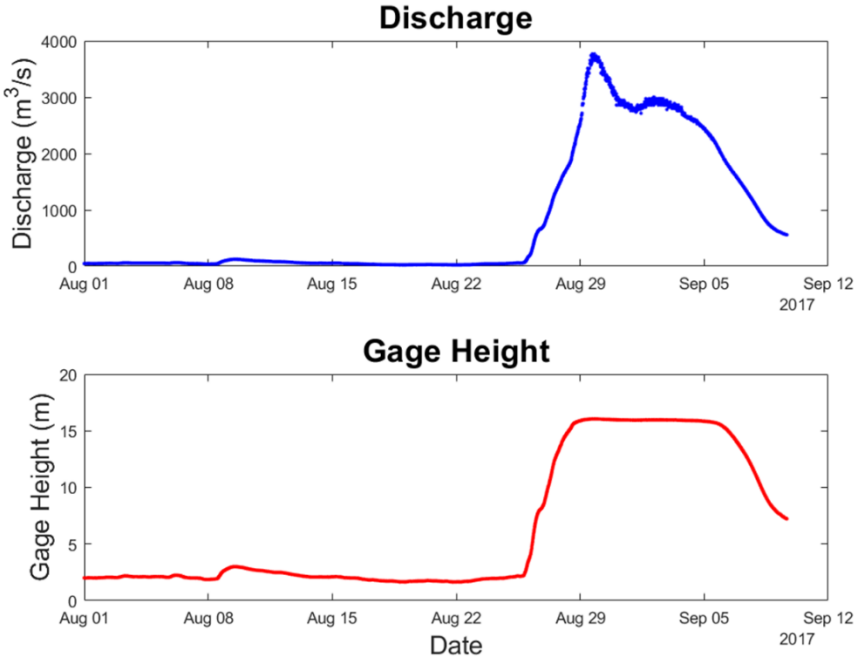

Figure 2 Brazos River Hydrographs. A) River discharge in cubic meters per second in blue. B) Gage Height in meters in red. Source: USGS

A new record discharge of 3,766.1 m3s-1 (Fig. 2) was reached by the substantial flooding due to Hurricane Harvey (Harvey). Harvey made landfall at Rockport, Texas as a Category 4 hurricane in August of 2017. The storm hovered over the Texas Coast for four days and delivered approximately 0.6 to 0.9 m of rainfall across the lower portion of the Brazos drainage basin (Fig. 3) (Blake & Zelinksy, 2018) and presumably resulted in the delivery of a significant sediment load to the Brazos Subaqueous Delta, as well as the north-western Gulf of Mexico (GOM).

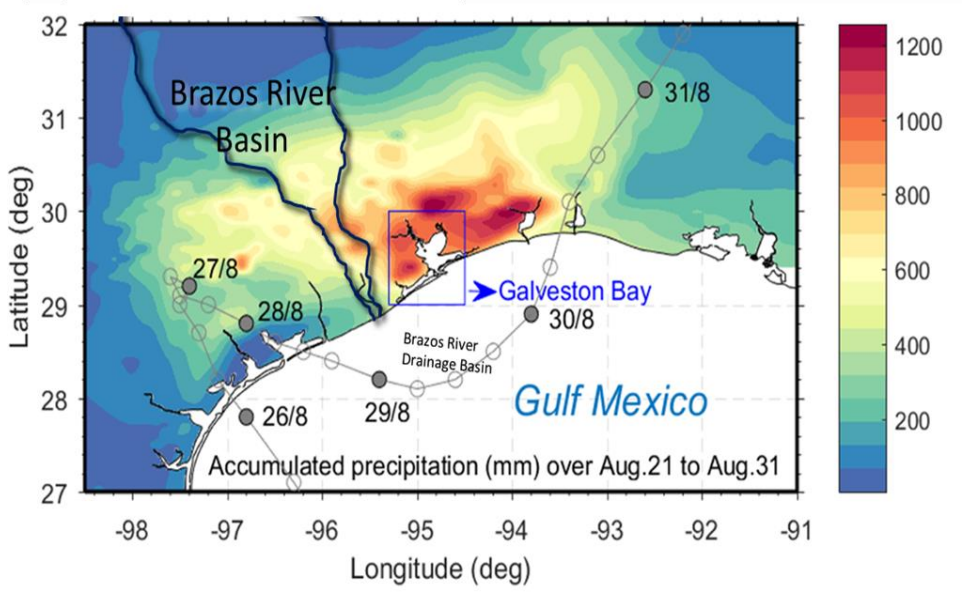

Figure 3 Harvey Accumulated Precipitation. Accumulated precipitation delivered by Hurricane Harvey from August 21, 2017 to August 31, 2017. The Brazos Drainage Basin is outlined in dark blue. Modified from: Du et al., 2019

This study focuses on delineating the Harvey Flood Deposit (HFD), assessing its initial volume, and then investigating the dispersal of sediment that constitutes the Harvey deposit, specifically, to determine the extent to which it was eroded and migrates because of the high-energy conditions of the winter months. It is hypothesized that the flood deposit was remobilized offshore and eventually ended up in the Texas Mud Blanket as previous research has observed (Carlin et al., 2021; McGuffin, 2018). Results from a time series of cores, beginning with a set of cores collected at peak discharge on September 10, 2017, followed by cruises conducted on October 10, 2017 and July 12, 2018, allow for the delineation and tracking of the dispersal and migration of this flood deposit.

1.1. Background

The Texas Coast is a microtidal, tropical region that receives 103.7 to 124.9 cm of rainfall annually (Rodriguez et al., 2000). Its longshore current flows from east to west but reverses at least once a year due to a change in wave direction in different seasons (Seelig and Sorensen, 1973). In Texas, droughts occur here more often than in other adjacent states due to processes between the GOM and Pacific (Fraticelli, 2006). When rainfall does occur, it typically does so as annual flash flooding events.

The winds flow southeasterly on average, but in the winter, ENs occur about 15 to 20 times per year (Rodriguez et al., 2000). These ENs consist of 3 parts: 1) the pre-frontal phase, when the wind is dominantly in the southerly direction and the atmosphere is typically warmer and more humid, 2) the frontal passage phase, when wind strength increases and the direction shifts from southerly to westerly, and 3) the post-frontal when wind direction switches in the northerly direction and the temperature and humidity drops (Moeller et al., 1993). EN frequency is enhanced during El Niño events, when, during the winter and early spring months, the southern United States experiences an increase in rainfall and storms. During this time, there is an increase in the number of floods occurring in the U.S. (Pizarro and Lall, 2002). The largest impact on the delta occurs when there is a drought period followed by a flood (Fraticelli, 2006). This is because the drainage basin soils are more susceptible to erosion due to the lack of living vegetation, allowing greater delivery of sediment to the river. In addition, there is a greater accumulation of sediment in the lower river, due to salt wedge trapping (Carlin et al., 2015), resulting in more sediment being flushed out to the delta during a major flood

event. This means that when there is a dry La Niña (where the Southern U.S. experiences a lack of rainfall), followed by a large El Niño, there is an increase in sediment deposited in the Brazos delta (Fraticelli, 2006). Since Harvey occurred during a La Niña event and resulted in the record discharge of the Brazos, the thickest flood deposit found on this delta was recorded (Hoelscher, 2018). Along with the increase in storms during El Niño, there is an increase in wave activity in the GOM. This increase in wave activity will cause resuspension and mobilization of the flood deposit to a new depocenter (Carlin et al., 2021).

The Brazos River is the 11th longest river in the United States, reaching about 1,352 km starting in northeastern New Mexico and ending on the Texas Coast near Freeport and spilling directly into the GOM. It has a watershed of about 118,000 km^2 and is one of two rivers that consistently drain directly into the GOM, the other being the Mississippi River, and the only one in Texas (Rodriguez et al., 2000). The river was diverted from its original location, NE from its current location, in 1929 and now drains out into the GOM to what we now know as the Brazos Delta. This delta is approximately 35 km^2, and about 70% of it is submerged, making it a subaqueous delta (Rodriguez et al., 2000).

It is estimated there is about 10 to 16 metric tons of sediment being delivered to the GOM every year by the Brazos, making it the second-largest sediment source for the GOM (Ludwig, 1998; Carlin, 2013). Despite this, the sedimentation from this river is largely driven by flood cycles (Rodriguez et al., 2000). Before a flood, the sediment of the Brazos gets trapped in the estuary due to the salt wedge that intrudes into the river (Carlin et al., 2014). When a flood occurs, the energy from the runoff is strong enough to

push the salt wedge out of the river and resuspend the trapped sediment (Carlin et al., 2014). This resuspended sediment has been observed to exit the mouth of the river in the form of a plume containing both hypopycnal and hyperpycnal flow (Carlin et al., 2013).

2. METHODS

2.1. Sampling Techniques

On September 10, 2017, a research cruise aboard the R/V Pelican went to the Brazos Delta and collected a series of 15 box cores across an established grid across the subaqueous delta (Fig. 4). From each box core, a 15 cm diameter subcore, a plexiglass x-ray tray, and an 8 cm diameter subcore were collected. Along with the box cores, Total Suspended Solids (TSS), salinity, temperature, and density were measured using a CTD rosette and a TSS Sensor that was attached to the CTD. To calibrate the CTD TSS measurements, TSS was also measured using a Millipore filtration system connected to a vacuum pump filtered through a 0.45-micron filter. The filter weight and initial volume was recorded along with the post filter weight and volume. These were used to calculate TSS in mg L^{-1}.

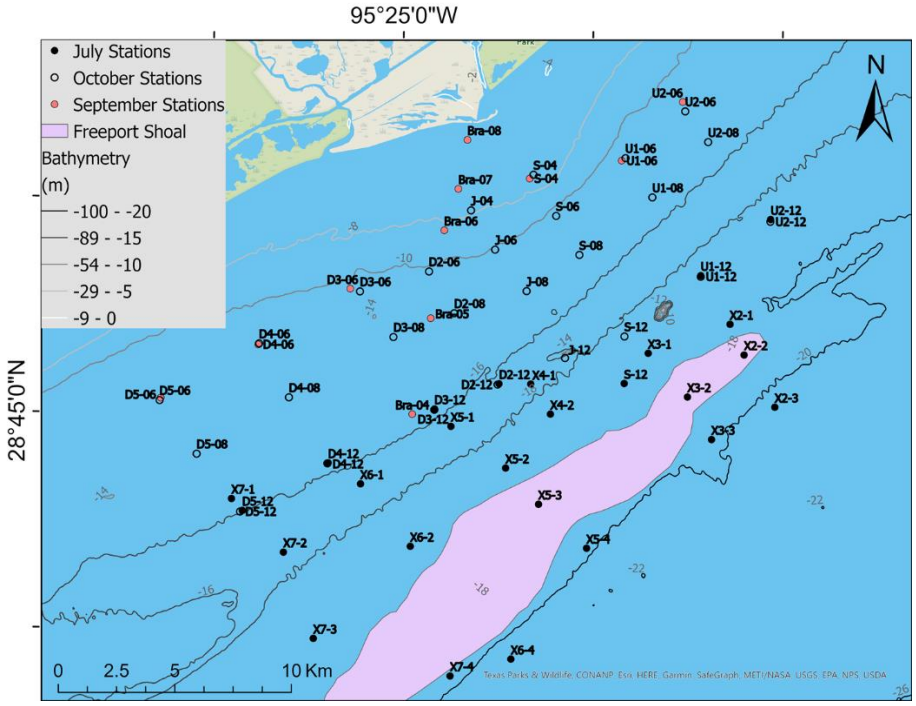

Figure 4 Project Station Locations. Note, the cores collected on the R/V Pelican in September 2017 are noted by a pink circle. The October 2017 and July 2018 cores collected by the R/V Trident are noted by a circle and a black circle. The Freeport Rocks are pink.

The 15 cm diameter subcore was sub-sectioned into 1-cm-thick slices and stored in sealed plastic bags until analysis. The x-ray tray was used to collect a digital x-radiograph to analyze sedimentary fabric. The 8 cm diameter subcore was archived intact for future analyses. Follow-up cruises aboard the R/V Trident were conducted on October 29, 2017 and July 12, 2018 to re-core the 2017 R/V Pelican cruise core sites and collect cores from the remainder of the grid sites and each box core was analyzed as previously described.

2.2. Grain Size Analysis

Sediment samples dispersed in a sodium hexametaphosphate ($Na_6[(PO_3)_6]$) solution were sieved through a 2 mm sieve. The <2 mm sediment fraction was placed into a Malvern Mastersizer 2000. This instrument uses laser diffraction to analyze grain sizes from clay (<0.002 mm) to sand (0.063-2000 mm). It provides a grain size distribution based on volume in the form of a percentage, and it also provides sediment statistics for each sample including kurtosis, Standard deviation, mean (Volume Weighted), and skewness.

2.3. Water Content

Water content was measured by putting a sample into a pre-weighed aluminum tin until a minimum mass of approximately 8 g was achieved. The tin and sample were weighed again, then baked in an oven at 70°C for 24 hours. The desiccated sample weight was recorded, and the percent water content was calculated.

2.4. Identifying the Hurricane Harvey Flood Deposit

To identify the Harvey Flood Deposit, water content, grain size data, and x-radiographs were analyzed (Fig. 5). In a storm deposit, the water content will typically be higher at the surface and decrease dramatically with depth (Wheatcroft et al., 1996). This is due to the fresh deposit being placed quickly, then being compacted as more sediment is deposited on top. (Wheatcroft et al., 1996). Grain size will have a gradient of either fining upward or coarsening upward (Wheatcroft, 2006). This is due to changes in the energy where the energy decreases and deposits the coarse grain sizes first then the fine, thus forming the fining upward trend. The coarsening upwards trend is due to the increase in the transport capacity of the river during flood events (Wheatcroft, 2006). X-

radiographs show the density variations in the sediment and any bioturbation that might be present. Since the HFD was deposited shortly before core collection, little if any bioturbation is expected. By combining these three factors, the thickness of the HFD at each site during each cruise can be recorded.

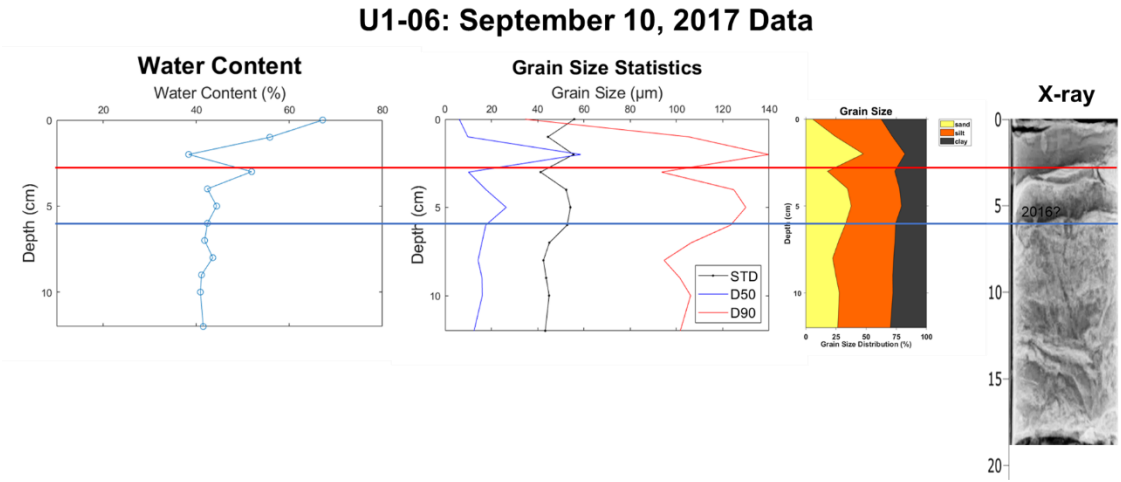

Figure 5 U1-06: September Data. The red line indicates where we believe the base of the Hurricane Harvey flood deposit is located. The blue line indicates where we believe the base of the 2016 flood deposit is located.

2.5. Mapping and Other Analysis

Three spreadsheets that contain the coordinates, site name, and Harvey deposit thickness for each cruise were used to make up the main data set for the isopach maps and to make the site points. Two polygons were created: one Brazos Delta polygon and one Freeport Rocks polygon. Both were manually determined, with the Brazos Delta polygon drawn based on the site locations and the Freeport Rocks traced from a NOAA nautical basemap. A Pre-Harvey continuous surface of 0 cm was made to set a baseline for “pre-Harvey” conditions.

Using ArcGIS, a model was created within ArcPro Model Builder to project each sampling site's coordinates (points) from each sampling event onto the map interface. The HFD thickness associated with these points was interpolated into a continuous raster surface using the Inverse Distance Weighted (IDW) separately. These surfaces were then clipped to the manually determined polygons to create an isopach map for each. The Cut Fill tool was applied to determine changes in volume between the established regions between each sampling event. This tool calculates volumetric changes between two surfaces (our isopach maps in this case) and identifies where material has been deposited or eroded. The output of this tool also yields net changes in the volume for the given study area. With this tool, we determined the total HFD volume that existed at the time of each cruise by subtracting each HFD thickness map from the "pre-Harvey" raster. This gave us the total volume for each sampling period. To determine how much sample was eroded, the calculated volumes were subtracted from each other. Note, the volume calculation is only focused on the study area. This means that if the HFD were to migrate outside of the study area, the volume would decrease as a result.

To determine the influence currents had on the remobilization of the HFD, a critical shear velocity (U*cr) estimation is required. The protocol for estimating critical shear velocity provided by Van Rijn et al. (2020) was used, where an average of the median diameter of 60 μm for the samples collected, an average water depth for the deposit of 20 m, were used to estimate an average U*cr of 30 cms^{-1}. This velocity represents the minimum velocity needed to resuspend sediment with a diameter of 60

μm. From now on, currents that exceed this critical shear velocity will be called high-velocity currents.

The frequency of events where the critical shear stress was exceeded was determined using surface current data that was compiled and analyzed (TABS Buoy Database Query, 09/01/17-07/12/18). Meteorological data from the Texas Automated Buoy System (TABS), queried from 09/01/17-07/12/18 (TABS Buoy System, 2017), contains wind speed, wind direction, air temperature, and current speed, was used to analyze the meteorological conditions that existed between the first cruise and the last. For these purposes, ENs were selected based on the direction of the wind. The meteorological data along with the current data were placed in a spreadsheet for analysis. Here, all the currents that exceeded 30 cms^{-1} were marked. All the times where the winds were blowing from the north, blowing from the SE, and times where a tropical storm was in the GOM were marked. From there, the total times dedicated for each event when there were high-velocity currents were calculated.

The surface current and meteorological data were plotted using MATLAB and analyzed to determine the frequency and nature of the ENs where the current speed exceeded 30 cms^{-1} from September 2017 to July 2018. A baseline of 30 cms^{-1} was plotted on the current speed graph for reference (Fig. 11).

The Semi-implicit Cross-scale Hydroscience Integrated System Model (SCHISM) modified for the Gulf of Mexico and the Texas Bays and Rivers (Du et al., 2019) was used for a shelf simulation of salinity. This model uses river discharge, atmospheric forcing, and boundary conditions to reproduce variations in water level,

salinity, temperature, and current velocity, and included the Brazos River discharge for Harvey to provide salinity simulation of the Brazos River and Galveston Bay from August 30, 2017, to September 10, 2017 (Du et al., 2019). The simulation was used in this project to determine the direction of the Brazos plume as it exited the river during Harvey.

To calculate the total sediment load that was delivered from August 25, 2017, when Harvey made landfall, to September 8, 2017, when the freshwater plume from the Brazos returned to pre-flood levels, the discharge rate of the Brazos River was retrieved from USGS. By using the Brazos River Rating Curve (Carlin et al., 2016) that was generated using historic Brazos discharge values the river discharge the daily sediment yield (metric tons day^{-1}) was estimated (Fig. 6). The daily sediment yield was summed up to give the total sediment yield delivered by Hurricane Harvey from August 25 to September 8.

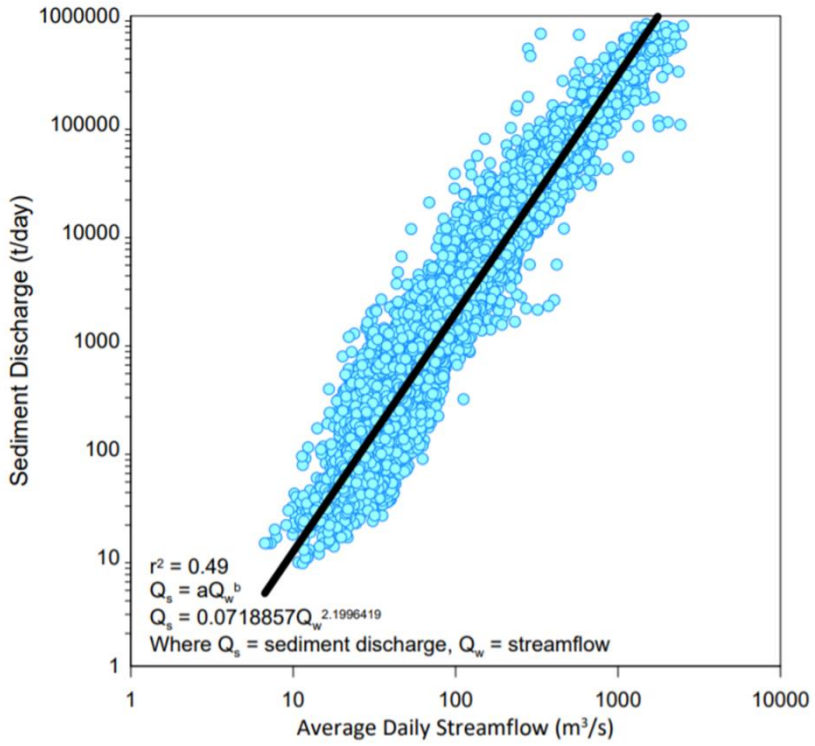

Figure 6 Rating Curve of Brazos River. This graph was created using historic sediment discharges and streamflow pulled from USGS. An equation was then determined using these values to convert Streamflow to Sediment Discharge (metric tons per day)

By using the volume calculations determined by ArcGIS Pro and using the average water content for the HFD, and the density of quartz (2.65 g cm^{-3}) for the average density of the sediment, the total mass of the HFD was found at each research cruise. By comparing the total mass found on the delta (HFD mass) to the total mass delivered during Harvey, the total mass that was lost and the total mass that was captured in the delta was determined.

3. RESULTS

3.1. Harvey Flood Deposit

The HFD was analyzed for all three research cruises. There was a total of 64 sites visited and a total of 62 cores analyzed. The cores were separated based on the cruise for which they were collected (i.e., September, October, or July).

On September 13, 2017, 11 cores were collected. The mean grain size class was 40.2 μm (silt), (Table 1). The overall grain size trend was a fining upwards trend. The September 2017 cores had an average water content of 43%, with the maximum reaching 53% and the minimum reaching 32% (Table 1). Water content was found to decrease with depth. It was determined that the September cores had an average storm deposit thickness of 5 cm, with a maximum of 12 cm and a minimum of 0 cm (Table 1).

Table 1 Sediment analysis for September 10, 2017 cores.

	Grain Size			Water Content			
	Trend	Depth (cm)	Mean Grainsize(μm)	Trend	Depth (cm)	Water content (%)	Storm layer (cm)
Mean	increase	3.1	40 (silt)	decrease	4.3	43.0	4.8 (+/-2)
Minimum	NA	0	9 (silt)	NA	0	32.4	0
Maximum	NA	9	253 (medium sand)	NA	10	53.1	12 (+/-2)
Median	NA	2	36 (silt)	NA	5	45.1	4 (+/-2)

On October 29, 2017, 24 cores were collected. The average grain size was also silt (30.2 μm) and had a coarsening upward trend (Table 2). Water content decreased downcore as well with an average of 44%, a maximum of 60.6%, and a minimum of

23% (Table 2). Analysis of the cores determined that the storm deposit has an average thickness of 4.8 cm, with a maximum of 12 cm and a minimum of 0 cm (Table 2).

Table 2 Sediment analysis for October 29, 2017 cores

	Grain Size			Water Content			
	Trend	Depth (cm)	Mean Grainsize (μm)	Trend	Depth (cm)	Water content (%)	Storm layer (cm)
Mean	decrease	3.3	30.2 (silt)	decrease	1.8	44.3	4.8 (+/-2)
Minimum	NA	0	7.4 (silt)	NA	0	23.4	0
Maximum	NA	15	225.6 (fine sand)	NA	12	60.6	12 (+/-2)
Median	NA	0	27.3 (silt)	NA	0	44.8	4.3 (+/-2)

The July 2018 trip resulted in the collection of 27 cores. The average grain size increased to 86.3 μm (very fine sand) (Table 3). The grain size trend for these cores was fining upward (Table 3). Water content decreased downcore, with an average water content of 42%, a maximum of 74%, and a minimum of 22.8% (Table 3). The storm deposit was analyzed to have an average thickness of 3 cm with a maximum of 11 cm and a minimum of 0 cm (Table 3).

Table 3 Sediment analysis for July 12, 2018 cores.

	Grain Size			Water Content			
	Trend	Depth (cm)	Mean Grainsize (μm)	Trend	Depth (cm)	Water content (%)	Storm layer (cm)
Mean	increasing	4.1	86.3 (very fine sand)	decrease	4.1	42.7	2.8 (+/-2)
Minimum	NA	0	7.7 (silt)	NA	0	22.8	0
Maximum	NA	11.0	566.8 (coarse sand)	NA	13.0	74.4	11.0 (+/-2)
Median	NA	4.0	76.0 (very fine sand)	NA	4.0	42.8	0

The southernmost stations in July 2018 did not have a flood deposit present and were composed of coarse sand, with some cores containing shell hash and extensive bioturbation (Fig. 7).

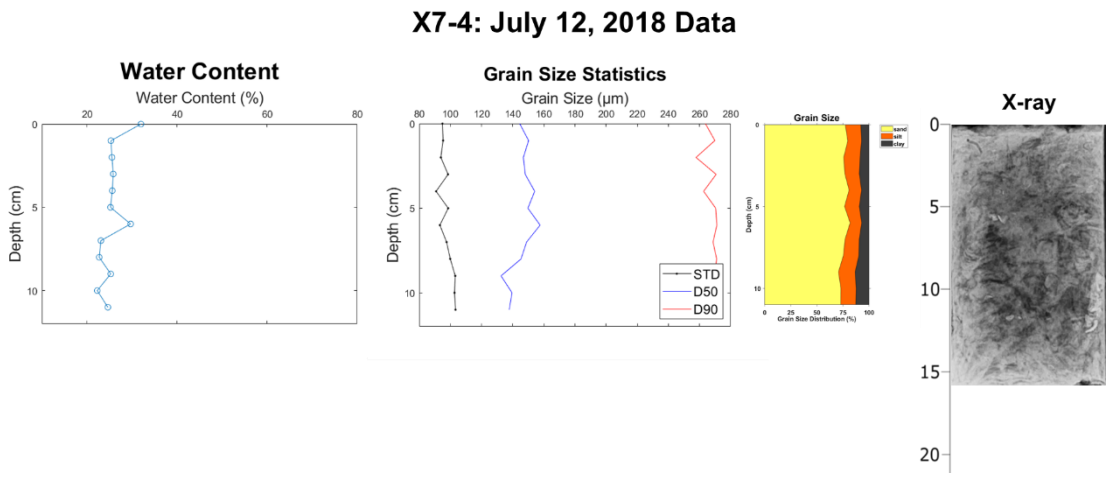

Figure 7 X7-4: July Data. This station was located behind the Freeport Rocks, which might explain the lack in Harvey Flood Deposit

3.2. Migration of the Flood Deposit

By using the Brazos River Rating curve, the total sediment yield for Hurricane Harvey was determined to be 24.5×10^6 metric tons of sediment. Transit profiles of salinity and TSS from data collected on September 10, 2017 are shown in Fig. 8.

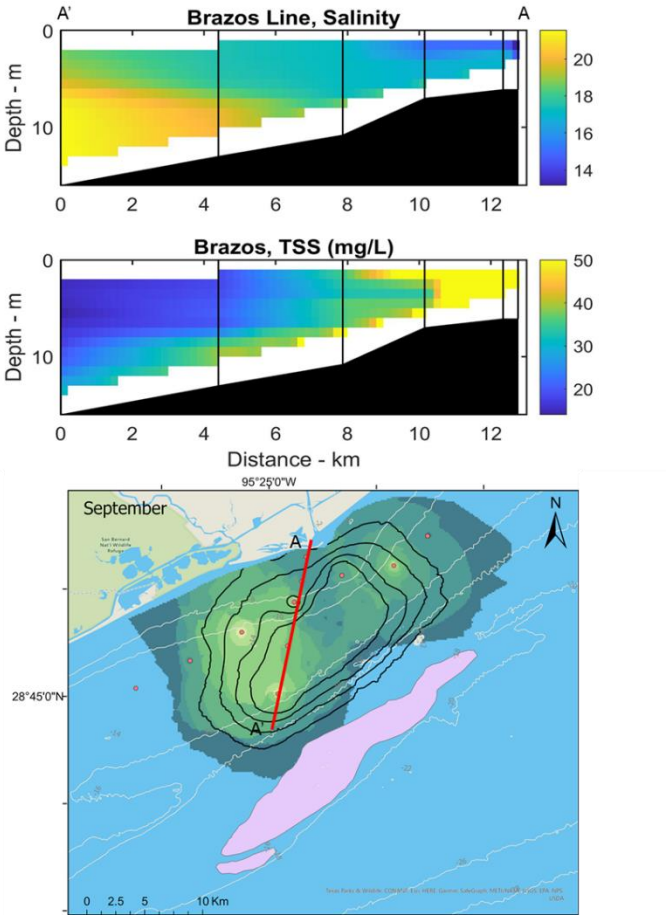

Figure 8 September CTD and TSS Data. A) Salinity and B) Total suspended solid data collected on September 10, 2017 compared to C) A sand concentration map of the HFD in September. A (located at station Bra-08) is closest inshore and A' (located at Bra-04) is furthest offshore

The TSS profile reveals both a buoyant hypopycnal plume and what appears to be a hyperpycnal plume, extending out to at least 8 km offshore. The relatively high sand content of 12% lends strong support to the idea that this is a hyperpycnal plume because it is doubtful that a buoyant plume would be able to transport sand that far offshore (Fig. 9).

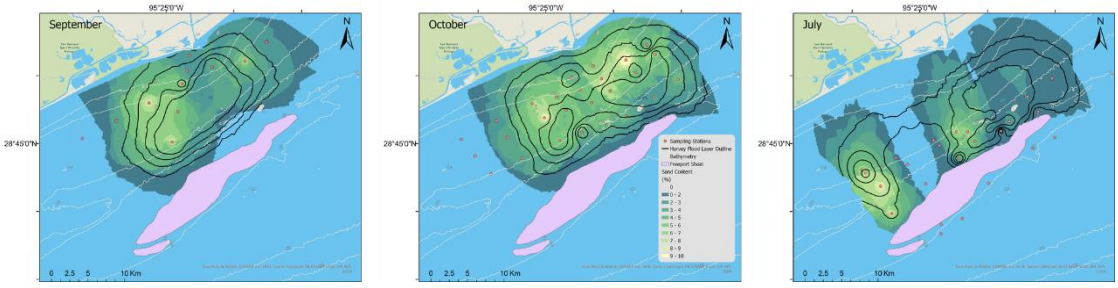

Figure 9 Sand Concentration of HFD. A) Sand concentration for September 2017, B) Sand concentration for October 2017, and C) Sand concentration for July 2018

The plume is shown to come out in two parts (yellow): a suspended plume more than likely consisting of clay and silt and a hyperpycnal plume most likely consisting of coarser grain sizes such as sand (Fig. 8).

The time series of isopach maps of the HFD show the aerial distribution of the deposit as discerned from the core data at each time step (Fig. 10). From the initial collection during September 10, 2017 to the second cruise on October 29, 2017, the HFD is seen to move to the east. From October 2017 to July 12, 2018, the movement of the deposit switches from an eastward movement to a westward one with an offshore migration as well (Fig. 10). It was determined based on the characteristics of the samples collected on and after the Freeport Rocks that the HFD did not surpass this shoal.

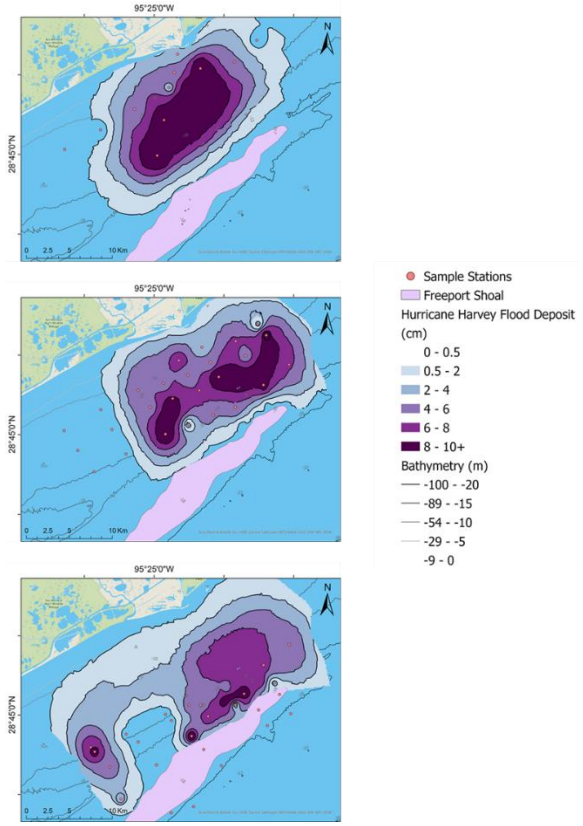

Figure 10 Hurricane Harvey Flood Deposit Thickness. A) September 2017, B) October 2017, and C) July 2018. Over all, there is a migration offshore and to the west with a barrier formed at the Freeport Rocks (pink).

The HFD volumes were calculated for each cruise using the isopach maps and the cut fill tool in ArcGIS Pro (Table 4). It was determined that the HFD volume on September 10, 2017 was 15.0×10^6 m^3, the total volume for October was 16.7×10^6 m^3, and the volume for July was 14.2×10^6 m^3 (Table 4). These volumes were used to determine the mass of the HFD, where it was found: a total of 17.1×10^6 metric tons of sediment made up the HFD in September, 19.5×10^6 metric tons of sediment made up the HFD in October, and 15.7×10^6 metric tons of sediment made up the HFD in July (Table 4).

Table 4 Harvey Flood Deposit Volume and Mass. Calculations for each cruise and the differences in volume and mass between each cruise.

Cruise	Volume (m^3)	Mass (metric Ton)
Total September	$15.0x10^6$	$17.1x10^6$
September to October	$1.7x10^6$	$2.4x10^6$
Total October	$16.7x10^6$	$19.5x10^6$
October to July	$2.5.x10^6$	$3.7x10^6$
Total July	$14.2x10^6$	$15.7x10^6$

They were compared amongst each other to determine the approximate volume of sediment gained or lost between each sampling period. Results show an increase in volume between September and October of $1.7x10^6$ m^3 (increase in mass $2.4x10^6$ metric tons) and a decrease in volume between October and July of $2.5.x10^6$ m^3 (decrease in mass of $3.7x10^6$ metric tons) (Table 4).

3.3. Meteorological Trends

Meteorological data was analyzed from September 2017 to July 2018 for extratropical storm events (Fig. 11). It was determined that during the study, there was potential extratropical activity for a total of 1,292.5 hours, with the first one beginning in September 2017 and the last one in April 2018. Of this, 279.5 hours occurred between the September and October cruise and 1,013 hours between the October 2017 cruise and the July 2018 cruise.

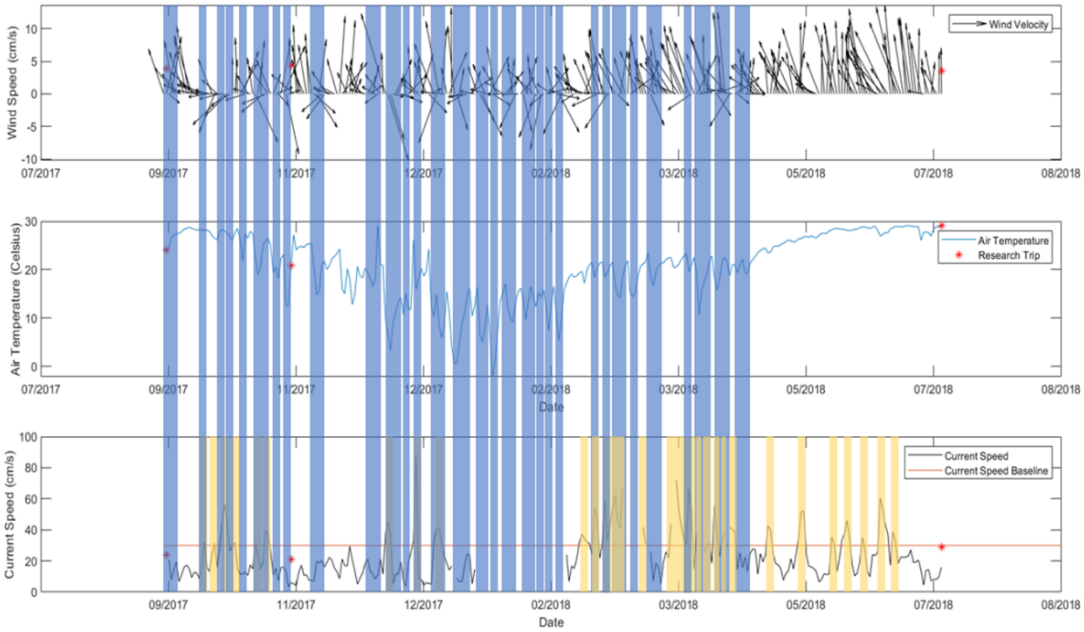

Figure 11 Meterological Data from September 2017 to July 2018. A) wind velocity (cm s^{-1}), B) air temperature, and C) current speed (cm s^{-1}). The red markers are when each cruise went out (September, October, and July). The red line on the last graph shows the minimum current speed required to resuspend silt (30 cm s^{-1}). The blue lines dictate extratropical northers, The yellow lines dictate a period when the current exceeded 30 cm s^{-1} (high-velocity current). Source: (TABS Buoy Database Query,09/01/17-07/12/18)

Analysis of the water current data, shown at the bottom of Fig. 11, reveals the total number of times high-velocity currents occurred was recorded for each month from September 10, 2017 to July 12, 2018 and graphed. There was a total of 672 hours of high-velocity currents. The average duration for these episodes was 60 hours (2.5 days), with a maximum of 216 hours (9 days) occurring twice in March 2018 and a minimum of 30 minutes occurring several times throughout the duration of the study (Table 5).

Table 5 High-Velocity Current Times. Red is the total time high-velocity currents occurred (from top to bottom) for Sept. 2017 to July 2018, Sept. 2017 to Oct. 2017, and Oct. 2017 to July 2018, green is only the times the high-velocity currents flowed to the west, blue is only the times the high-velocity currents flowed to the east, grey is the total times an extratropical norther (EN) event occurred.

	High-Velocity Currents (hr)	Westward High-Velocity Currents (hr)	Eastward High Velocity Currents (hr)	Extratropical Events (hr)
Total	672	500.5	171	1292.5
September to October	116	89	26.5	279.5
October to July	556	411.5	144.5	1,013

Of the total high-velocity time, 116 hours occurred between September 10, 2017 and October 29, 2017, and 556 hours occurred between October 29, 2017 and July 12, 2018. A total of 258.5 hours occurred during extratropical activity, making the time that high-velocity currents occurred during an EN about 61% of the total time (Fig. 11, Fig. 12).

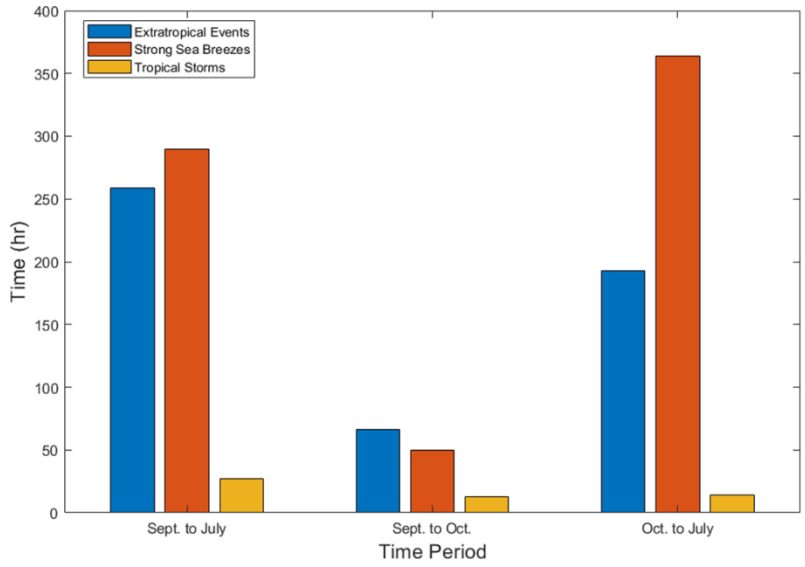

Figure 12 High-Velocity Current Times during Various Weather Phenomena. This figure shows the total amount of time High-Velocity Currents occur during Extratropical events (Blue), Strong Sea Breezes (orange), and Tropical Storms (yellow). They are separated into three time periods: the total sampling time (Sept. to July), from the first cruise to the second (Sept. to Oct.), and from the second cruise to the last (Oct. to July).

Between September 10, 2017 and October 29, 2017, for the high-velocity current events, 76.7% of the time the currents were flowing towards the west and 22.8% of the time the currents were flowing towards the east. During October 29, 2017 and July 12, 2018, the high-velocity currents moved to the west 74% of the time and flowed to the East 26% of the time (Table 5). The maximum speed reached was 88 cms^{-1} and the minimum was 3.2 cms^{-1}.

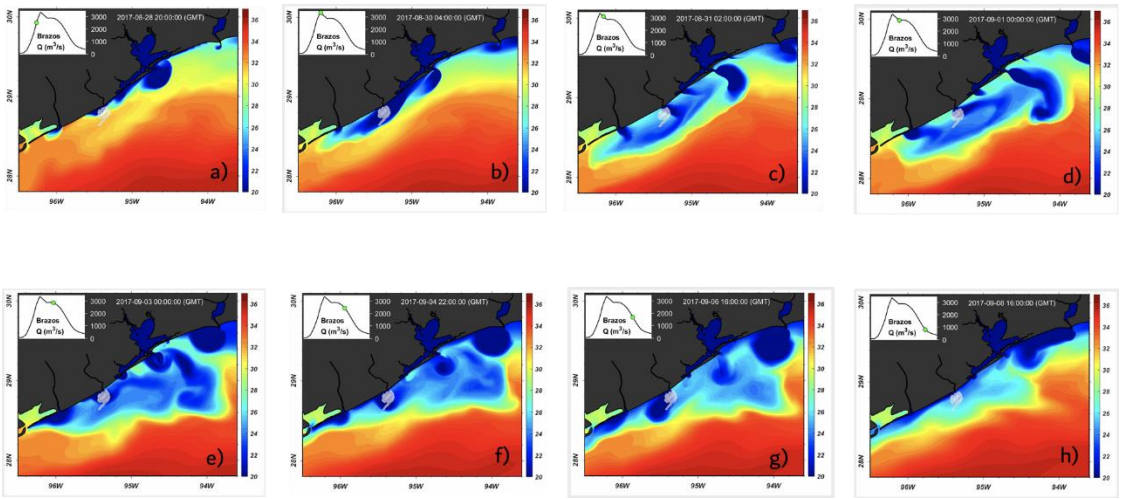

Figure 13 Freshwater input into the GOM from August 28, 2017 to September 8, 2017. The top left of each figure shows the discharge rate of the Brazos River at the time stamp shown next to it.

The SCHISM model output (Fig. 13) shows that the plume first entered the Gulf on August 28, 2017 (Fig. 13A), when Harvey stalled over the Texas coast (Blake and Zelinsky, 2018). The Brazos plume was flowing towards the west in the GOM, generally within 10 km or less from the coast. As peak discharge was reached on August 30, 2017 (Fig. 13B), and on August 31, 2017, the longshore currents shifted to an eastward flow, as the surface plume migrated from westward to eastward flow it extended up to 40 km

offshore, due south of the mouth of the river (Fig. 13C). Between August 31, 2017 and September 4, 2017, when the river experienced its prolonged high discharge period, the plume shifted back and forth between a westerly and easterly direction, resulting in the plume generally being oriented due south of the river offshore and along the coast west of the river mouth nearshore, generally within 9 km of the coast or less (Fig. 13C-13F). The plume continues to flow generally towards the east for 5 days, and then on September 5, 2017, as the decrease in the discharge rate of the river continued, the currents switched back to a westward flow direction (Fig. 13G).

4. DISCUSSION

Based on the hydrograph (Fig. 2) and the meteorological data (Fig. 11), the flooding of the Brazos began on August 25, 2017. An observable buoyant/hypopycnal plume first entered the GOM on August 27, 2017 where it flowed approximately 22 km to the southwest of the mouth of the river (Fig. 13A). This flood event caused the Brazos to reach a record discharge of 3,766 m^3s^{-1} on August 29, 2017 (Fig. 2). On August 30, 2017, the surface plume distance increased to approximately 70 km to the southwest of the mouth (Fig. 13B). As the floodwater pushed the saltwedge from within the lower river, to offshore of the river's mouthbar, it also transported the sediment that was previously trapped within the estuarine portion of the lower river to the subaqueous delta. This sediment transport occurred both within a buoyant hypopycnal plume as well as a hyperpycnal gravity flow (Fig. 8). Warrick and Milliman (2003) suggest that, when hyperpycnal flow exists, up to 75% of the sediment derived from floods can be transported to the shelf via hyperpycnal flow and that the hyperpycnal plume can transport sediment further offshore than the hypopycnal plume (Geyer et al., 2014). The distribution of the initial HFD does not precisely match the surface plume trend, however, it is speculated that it may better match the hyperpycnal flow trend which was likely the primary mechanism of initial sediment dispersal.

On August 31, 2017, longshore currents switched from westward to eastward flow, causing the buoyant surface plume to flow approximately 40 km to the east of the mouth, creating the initial easternmost flood deposits (Fig. 13C). On September 5, 2017, the currents shifted back towards the west, forcing the plume to flow to the west of the

mouth, and depositing Harvey sediment to the west (Fig.13F). Finally, on September 8, 2017, the plume dissipated (Fig. 13H). It was estimated that 24.5x10^6 metric tons of sediment was delivered to the GOM from August 25, 2017 to September 8, 2017, when the river discharge returned to a consistent low flow stage.

The first sampling trip occurred two days after the plume exited the GOM on September 10, 2017. It was found that the initial deposit formed about 10 km off the mouth of the river as a 10 cm thick deposit, with the thickest being about 12 cm. It was estimated that about 70% of the sediment that was delivered to the GOM was captured by the Brazos Delta as of September 10, 2017, meaning that 30% was diverted outside of the subaqueous delta sampling area. It is possible that the deposit was still forming when the trip was conducted given the results of the TSS diagram (Fig. 8) where hypopycnal and hyperpycnal plumes were captured. This explains why there was a net gain in HFD of 17.2x104 m^3 from September 10, 2017 to October 29, 2017 (Table 4), with a new volumetric estimate of 16.7x105 m^3 being formed for October 29, 2017.

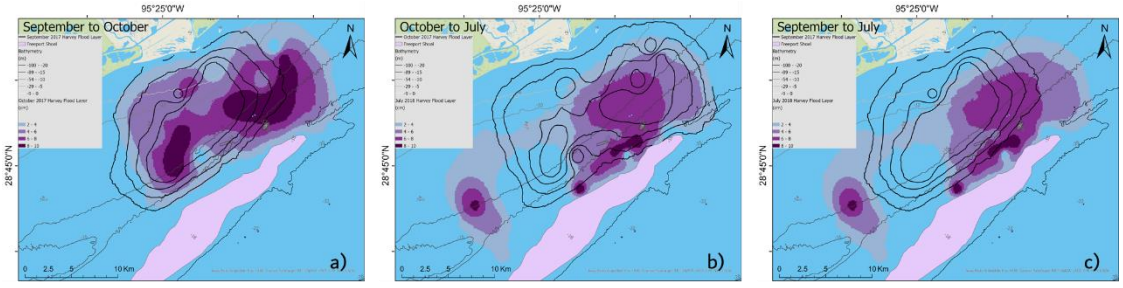

Figure 14 HFD Comparison. Locational difference between the Harvey Layer in: a) September 2017(black outline) to October 2017 (purple), b) October 2017 (black outline) to July 2018 (purple), and c) September 2017 (black outline) to July 2018 (purple).

From September and October, the deposit was remobilized about 10 km to the southeast from its initial deposition site (Fig. 14A). The movement of the deposit is toward the southeast of the delta from September 10, 2017 to October 29, 2017 (Fig. 10 & 14A), with a net loss in the center of the sample area. During this time, there is also a net overall gain of sediment. This is likely due to the first sampling period occurring so soon after peak discharge, so the HFD was still being deposited post-September 10, 2017 cruise. A total of 80% of the sediment that was delivered was captured by the delta as of October 29, 2017, making the other 20% lost to the GOM. We speculate that much of this sediment was ultimately transported toward the southwest, towards the TMB. Carlin et al., (2020) found that within the TMB, at a site 92 km towards the southwest, that flood deposits from smaller floods from 2015 and 2016 produced deposits as thick as 11 cm within one year of the flood, a deposit of comparable thickness to that found within the subaqueous delta proximal to the mouth of the Brazos, suggesting significant and rapid sediment transport to this distal depocenter.

The July 12, 2018-HFD deposit (Fig. 9C) reveals that from October 29, 2017 to July 12, 2018, the HFD depo-center migrated about 10 km in the southwest direction (Fig. 10 & 14B). The southern and offshore-ward limit of the HFD is demarcated by Freeport Rocks, a relict, Holocene-aged oyster reef (Winchester, 1971), which shoals to 2-3 m shallower than surrounding seabed and consist of largely of shell gravel with abundant partially lithified hard bottom. The Freeport Rocks appear to have acted as a barrier to sediment transport. During the time between the October 29, 2017 and the July 12, 2018 cruises, the HFD decreased from 16.7x106 m^3 to 14.1x106 m^3, representing a

15% loss in volume (Table 4). A total of 279.5 hours occurred during EN activity between the September 10, 2017 and October 29, 2017 cruises (Fig. 12), where there was a total of 116 hours of high-velocity current activity (Table 5). Of the 116 hours, 56.9% occurred during an extratropical event. The current switched directions a total of 49 times, where 22.8% of the 116 hours the current flowed east and 89% flowed west. The two lobes within October 29, 2017, indicate bifurcation of the deposit as well as westward migration since September 10, 2017. The bifurcation of the deposit is likely the result of the "jet" flow out of the mouth of the Brazos as the discharge entered the GOM. Collectively, these changes are also indicative of the transport of the HFD after initial deposition.

Between October 29, 2017 and July 12, 2018 the currents reach high velocities a total of 556 hours. Of the 556 hours, 74% of the time the current was flowing to the west and 26% was flowing to the east (Table 5). Of the 556 hours, 34.6% occurred during an extratropical event (Fig. 12). There was a loss of 25.3×10^4 m^3 of the HFD, representing a 15% volume change. About 79% of the sediment that was delivered was captured by the delta, making 21% lost to the GOM. Fig. 10C shows the July 12, 2018 deposit has two prominent lobes and that the deposit has been significantly bifurcated with the two lobes separated by 6 km, with the bed between the lobes devoid of HFD sediment, indicating sediment bypass coupled with erosion. There does not appear to be any additional eastward migration of the deposit. The 15% loss in volume change likely resulted from westward migration towards the Texas Mudbelt, outside of the sample area, which is supported by the total mass lost in July.

The question of the driving force of this migration still stands. After observing the meteorological data, it was determined that there were 258.5 hours when the currents exceeded the minimum velocity during an EN event. That comes up to 61% of the time the currents exceeded 30 cms^{-1}. This forms a new question: What caused the other high currents to occur? During September 10, 2017 to July 12, 2018 sampling period, there were a total of three tropical storms that entered the GOM. There is a possibility that the wind from these storms could have affected about 5% of the currents at the sampling site, for 20 hours of the 672 total hours of high-velocity currents occurred during the time a tropical storm entered the GOM. The rest of the high-velocity currents were more than likely affected by strong sea-breezes given that of the other 413.5 hours when the currents exceeded the minimum velocity with no influence from ENs or tropical storms, 70% had winds traveling from the southeast direction, which implies the wind was moving from sea to land. In conclusion, potential drivers for the migration of the deposit could be a combination of extratropical events and sea breezes.

The U*cr estimation does not consider any physical characteristics of the seafloor that might affect the shear stress such as seafloor roughness, it is just a rough approximation, but is the best approximation available. The same can be said for the estimation of bottom currents based on surface currents. About 13% of the surface current and meteorological data were missing due to sensor malfunction. Regarding the interpretation of the distributions of the HFD, the interpolated maps are our best interpretation of the distribution of the HFD with available data.

5. CONCLUSIONS

This analysis showed the movement of the HFD over the span of one month in late fall then nine months from late fall to mid-summer. A total of $24.5x10^6$ metric tons of sediment was delivered to the GOM due to Hurricane Harvey. The changing of the flood deposit thickness from September 10, 2017 to July 12, 2018 shows that the HFD has been remobilized and redeposited further offshore, has bifurcated, and a portion of the deposit has migrated 10 km to the west over the course of the 10 months. It is believed that the area that has the largest loss of Harvey sediment is the initial deposition site.

On September 10, 2017, 69% of the total sediment yield was captured by the Brazos Subaqueous Delta. The other 31% was transported toward the TMB outside the study area or was still suspended in the water column. The captured material increased to 79% on October 29, 2017 due to the sediment still being deposited. The other 21% was transported to the TMB outside the study area. On July 12, 2018, 64% of the sediment was captured by the delta, which indicates that 36% was remobilized and/or transported to the TMB.

From September 10, 2017 to October 29, 2017, the flood deposit was remobilized to the southeast of the mouth. It is speculated that the divergence in the flood deposit that is observed from the October 29, 2017 cruise and the July 12, 2018 cruise is due to the "jet" flow of the river. Overall, the movement of the deposit was offshore and to the West, towards the TMB, which corresponds with what was previously observed. The Harvey deposit was also reworked and remobilized across the

shelf during the winter portion of the study due to extratropical storm passage, with additional remobilization due to strong sea-breezes. It was expected for the deposit to completely distribute southward (offshore), into the GOM, but the southernmost stations tell a different story. Freeport Rocks appear to have prevented the deposit from migrating further offshore, based on the lack of Harvey sediment in the southernmost stations. It is speculated that the portion of the HFD that is being eroded is continuing to be remobilized toward the TMB as a distal depocenter.

When the sediment is re-suspended and transported away from the initial depositional site, the associated organic matter, particle-bound contaminants, and nutrients are also re-suspended and re-introduced into the water column. With each re-suspension event, the seabed is re-oxygenated, allowing the stored organic matter to be oxidized, degraded, and consumed.

Although the degradation/transformation of organic matter is highly studied, the flux of nutrients and the fate and transport of the particle-bound contaminants are not specifically addressed. Inferences can be made about this process, but knowing the timing and the depth of resuspension, as well as the flux of the flood deposit as it migrates across the shelf, will help support these inferences.

REFERENCES

Anderson, J. B., Rodriguez, A. B., Abdulah, K., & Fillon, R. (2004). Late Quaternary Stratigraphic Evolution of the Northern Gulf of Mexico Margin: A Synthesis Experimental Sequence Stratigraphy I Vie

Anderson, J. B., Wallace, D. J., Simms, A. R., Rodriguez, A. B., Weight, R. W. R., & Taha, Z. P. (2016). Recycling sediments between source and sink during a eustatic cycle: Systems of late Quaternary northwestern Gulf of Mexico Basin. In Earth-Science Reviews (Vol. 153, pp. 111–138). Elsevier B.V. https://doi.org/10.1016/j.earscirev.2015.10.014

Banfield, L. A., & Anderson, J. B. (2004). Late quaternary evolution of the Rio Grande delta: complex response to eustasy and climate change. Society for Sedimentary Geology, 79, 289–306. https://archives.datapages.com/data/sepm_sp/SP79/Late_Quaternary_Evolution_of_the_Rio_Grande_Delta.htm

Bianchi, T. S., Mitra, S., & McKee, B. A. (2002). Sources of terrestrially-derived organic carbon in lower Mississippi River and Louisiana shelf sediments: Implications for differential sedimentation and transport at the coastal margin. *Marine Chemistry*, *77*(2–3), 211–223. https://doi.org/10.1016/S0304-4203(01)00088-3

Bianchi, T. S., Galler, J. J., & Allison, M. A. (2007). Hydrodynamic Sorting and Transport of Terrestrially Derived Organic Carbon in Sediments of the Mississippi and Atchafalaya Rivers. *Estuarine, Coastal and Shelf Science*, *73*(1–2), 211–222. https://doi.org/10.1016/j.ecss.2007.01.004

Blake, E., & Zelinsky, D. A. (2018). Tropical Cyclone Report: Hurricane Harvey. In *Noaa/nhc*. https://www.nhc.noaa.gov/data/tcr/AL092017_Harvey.pdf

Carlin, J. A. (2013). Sedimentation of the Brazos River System: Storage in the Lower River , Transport To the Shelf and the Evolution of a Modern Subaqueous Delta (Issue August) [Texas A&M University]. https://hdl.handle.net/1969.1/151110

Carlin, J. A., & Dellapenna, T. M. (2014). Event-driven deltaic sedimentation on a low-gradient, low-energy shelf: The Brazos River subaqueous delta, northwestern Gulf of Mexico. *Marine Geology*, *353*, 21–30. https://doi.org/10.1016/j.margeo.2014.03.017

Carlin, J. A., Dellapenna, T. M., Strom, K., & Noll, C. J. (2014). The Influence of a Salt Wedge Intrusion on Fluvial Suspended Sediment and the Implications for Sediment

Transport to the Adjacent Coastal Ocean: A Study of the Lower Brazos River TX, USA. *Marine Geology*. https://doi.org/10.1016/j.margeo.2014.11.001

Carlin, J. A., & Dellapenna, T. M. (2015). The evolution of a subaqueous delta in the Anthropocene: A stratigraphic investigation of the Brazos River delta, TX USA. *Continental Shelf Research*, *111*, 139–149. https://doi.org/10.1016/j.csr.2015.08.008

Carlin, J. A., Lee, Guan-hong, Dellapenna, T. M., & Laverty, P. (2016). Sediment Resuspension by Wind, Waves, and Currents During Meteorological Frontal Passages in a Micro-Tidal Lagoon. *Estuarine, Coastal and Shelf Science*, *172*, 24–33. https://doi.org/10.1016/j.ecss.2016.01.029

Carlin, J. A., Schreiner, K. M., Dellapenna, T. M., McGuffin, A. B., & Smith, R. W. (2021). Evidence of Recent Flood Deposits within a Distal Shelf Depocenter and Implications for Terrestrial Carbon Preservation in Non-deltaic Shelf Settings. *Marine Geology*, *431*, 106376. https://doi.org/10.1016/j.margeo.2020.106376

Coleman, J. M., & Prior, D. B. (1982). Deltaic Environments of Deposition. *AAPG Memoir*, *31*, 139–178. http://archives.datapages.com/data/specpubs/sandsto2/data/a058/a058/0001/0100/0139.htm

Du, J., & Park, K. (2019). Estuarine salinity recovery from an extreme precipitation event: Hurricane Harvey in Galveston Bay. Science of the Total Environment, 670, 1049–1059. https://doi.org/10.1016/j.scitotenv.2019.03.265

Feng, H., Cochran, J. K., Lwiza, H., Brownawell, B. J., & Hirschberg, D. J. (1998). Distribution of Heavy Metal and PCB Contaminants in the Sediments of an Urban Estuary: The Hudson River. *Marine Environmental Research*, *45*(1), 69–88. https://doi.org/10.1016/S0141-1136(97)00025-1

Fraticelli, C. M. (2006). Climate Forcing in a Wave-Dominated Delta : The Effects of Drought – Flood Cycles on Delta Progradation. *Sedimentary Research*, *76*, 1067–1076. https://doi.org/10.2110/jsr.2006.097

Geyer, W. R., Hill, P. S., & Kineke, G. C. (2004). The Transport, Transformation and Dispersal of Sediment by Buoyant Coastal Flows. *Continental Shelf Research*, *24*(7–8), 927–949. https://doi.org/10.1016/j.csr.2004.02.006

Goni, M. A., Ruttenberg, K. C., & Eglinton, T. I. (1997). Sources and Contribution of Terrigenous Organic Carbon to Surface Sediments in the Gulf of Mexico. *Nature*, *389*(6648), 275–278. https://doi.org/10.1038/38477

Hguyen, D. N. (2017). View of Effects of ENSO on cold-air activities and tropical cyclones in Vietnam. Vietnam Journal of Science, Technology and Engineering, 59(2), 88–91. https://vietnamscience.vjst.vn/index.php/VJSTE/article/view/48/50

Hoelscher, Christena Elizabeth (2018). How Does the Hurricane Harvey Deposits Compare to Past Brazos Subaqueous Delta Flood Deposits. Undergraduate Research Scholars Program. Available electronically from https : / /hdl .handle .net /1969 .1 /188547.

Jones, G. R., Nash, J. D., Doneker, R. L., & Jirka, G. H. (2007). Buoyant Surface Discharges into Water Bodies. I: Flow Classification and Prediction Methodology. *Journal of Hydraulic Engineering*, *133*(9), 1010–1020. https://doi.org/10.1061/(ASCE)0733-9429(2007)133:9(1010)

Kineke, G. C., Woolfe, K. J., Kuehl, S. A., Milliman, J. D., Dellapenna, T. M., & Purdon, R. G. (2000). Sediment Export from the Sepik River, Papua New Guinea: Evidence for a Divergent Sediment Plume. *Continental Shelf Research*, *20*(16), 2239–2266. https://doi.org/10.1016/S0278-4343(00)00069-8

Kniskern, T. A., Mitra, S., Orpin, A. R., Harris, C. K., Walsh, J. P., & Corbett, D. R. (2014). Characterization of a flood-associated deposit on the Waipaoa River shelf using radioisotopes and terrigenous organic matter abundance and composition. Continental Shelf Research, 86(C), 66–84. https://doi.org/10.1016/j.csr.2014.04.012

Kuehl, S. A., Brunskill, G. J., Burns, K., Fugate, D., Kniskern, T., & Meneghini, L. (2004). Nature of Sediment Dispersal off the Sepik River, Papua New Guinea: Preliminary Sediment Budget and Implications for Margin Processes. *Continental Shelf Research*, *24*(19), 2417–2429. https://doi.org/10.1016/j.csr.2004.07.016

Ludwig, W., & Probst, J.-L. (1998). River Sediment Discharge to the Oceans: Present-Day Controls and Global Budgets. *American Journal of Science*, *298*, 265–295.

Ludwig, W., Dumont, E., Meybeck, M., & Heussner, S. (2009). River Discharges of Water and Nutrients to the Mediterranean and Black Sea: Major Drivers for Ecosystem Changes During Past and Future Decades. In *Progress in Oceanography* (Vol. 80, Issues 3–4, pp. 199–217). Pergamon. https://doi.org/10.1016/j.pocean.2009.02.001

McGuffin, Andrew Brian (2018). Brazos River Flood Sediment Deposition, Remobilization and Continental Shelf Pathways. Master's thesis, Texas A & M University. Available electronically from https : / /hdl .handle .net /1969 .1 /173486.

McKee, B. A., Aller, R. C., Allison, M. A., Bianchi, T. S., & Kineke, G. C. (2004). Transport and Transformation of Dissolved and Particulate Materials on Continental Margins Influenced by Major Rivers: Benthic Boundary Layer and Seabed Processes. *Continental Shelf Research*, *24*(7–8), 899–926. https://doi.org/10.1016/j.csr.2004.02.009

Milliman, J. D., & Meade, R. H. (1983). World-wide Delivery of Sediment to the Oceans. *Journal of Geology*, *91*(1), 1–21. https://doi.org/10.1086/628741

Millman, J. D., & Farnsworth, K. L. (2011). *River Discharge to the Coastal Ocean: A Global Synthesis*. Cambridge University Press.

Moeller, C. C., Huh, O. K., Roberts, H. H., Gumley, L. E., & Menzel, W. P. (1993). Response of Louisiana Coastal Environments to a Cold Front Passage. Journal of Coastal Research, 9(2), 434–447. https://www.jstor.org/stable/4298101?seq=1#metadata_info_tab_contents

Nittrouer, C. A., & Wright, L. D. (1994). Transport of Particles Across Continental Shelves. *Reviews of Geophysics*, *32*(1), 85. https://doi.org/10.1029/93RG02603

Nittrouer, C. A., Kuehl, S. A., Figueiredo, A. G., Allison, M. A., Sommerfield, C. K., Rine, J. M., Faria, L. E. C., & Silveira, O. M. (1996). The geological record preserved by Amazon shelf sedimentation. Continental Shelf Research, 16(5–6), 817–841. https://doi.org/10.1016/0278-4343(95)00053-4

Palinkas, C. M. (2009). The Timing of Floods and Storms as a Controlling Mechanism for Shelf Deposit Morphology. Journal of Coastal Research, 255(255), 1122–1129. https://doi.org/10.2112/08-1041.1

Piechota, T. C., & Dracup, J. A. (1996). Drought and Regional Hydrologic Variation in the United States: Associations with the El Nino-Southern Oscillation. In *WATER RESOURCES RESEARCH* (Vol. 32, Issue 5). https://doi.org/10.1029/96WR00353

Pizarro, G., & Lall, U. (2002). El Nino-induced Flooding in the U.S. West: What Can We Expect? *Eos*, *82*(32), 349–352.

Roberts, H. H., Huh, O. K., Hsu, S. A., Rouse, L. J., & Rickman, D. (1987). IMPACT OF COLD-FRONT PASSAGES ON GEOMORPHIC EVOLUTION AND SEDIMENT DYNAMICS OF THE COMPLEX LOUISIANA COAST. Faculty Publications, 2. https://digitalcommons.lsu.edu/geo_pubs/1721

Rodriguez, A. B., Hamilton, M. D., & Anderson, J. B. (2000). Facies and Evolution of the Modern Brazos Delta , Texas : Wave Versus Flood Influence. *Sedimentary*

Research, 70(2), 283–295. https://doi.org/10.1306/2DC40911-0E47-11D7-8643000102C1865D

Seelig, W. N., & Sorensen, R. M. (1973). *Investigation of Shoreline Changes at Sargent Beach, Texas*.

Shideler, G. L. (1978). A sediment-dispersal model for the South Texas continental shelf, northwest Gulf of Mexico. Marine Geology, 26(3–4), 289–313. https://reader.elsevier.com/reader/sd/pii/0025322778900646?token=FC69192FC7643EDECFEE32F82C3BF206800A03840FBE8AEB04D30886AC1BA0A3AD39C6973E03BBBB41EC3B8EF9CCA58B&originRegion=us-east-1&originCreation=20210617213540

TABS Buoy Database Query page. (2017). https://tabs.gerg.tamu.edu/tglo/tabsqueryform.php?buoy=B

USGS. (2016). USGS Current Conditions for USGS 08116650 Brazos Rv nr Rosharon, TX. https://nwis.waterdata.usgs.gov/usa/nwis/uv/?cb_00060=on&format=gif_stats&site_no=08116650&period=&begin_date=2016-05-29&end_date=2016-07-29

USGS. (2017). USGS Current Conditions for USGS 08116650 Brazos Rv nr Rosharon, TX. https://nwis.waterdata.usgs.gov/nwis/uv?cb_00060=on&format=gif_stats&site_no=08116650&period=&begin_date=2016-05-29&end_date=2017-09-10

van de Giesen, N. (2020). Human Activities have Changed the Shapes of River Deltas. In *Nature* (Vol. 577, Issue 7791, pp. 473–474). Nature Research. https://doi.org/10.1038/d41586-020-00047-y

Van Rijn, L. C. (2020). Literature review of critical bed-shear stress for mud-sand mixtures. 1–56. https://www.leovanrijn-sediment.com/papers/Threshsandmud2020.pdf

Wadsworth, A. H., Jr. (1966). Historical Deltation of the Colorado River, Texas. Deltas in Their Geologic Framework, 99–105. http://archives.datapages.com/data/hgssp/data/016/016001/99_hgs0160099.htm

Warrick, J.A. and Milliman, J.D., 2003. Hyperpycnal sediment discharge from semiarid southern California rivers: Implications for coastal sediment budgets. Geology, 31(9), pp.781-784.

Weight, R. W. R., Anderson, J. B., & Fernandez, R. (2011). Rapid Mud accumulation on the central Texas shelf linked to climate change and sea-level rise. Journal of Sedimentary Research, 81(10), 743–761. https://doi.org/10.2110/jsr.2011.57

Wheatcroft, R. A., Sommerfield, C. K., Drake, D. E., Borgeld, J. C., & Nittrouer, C. A. (1997). Rapid and widespread dispersal of flood sediment on the northern California margin. Geology, 2(25), 163–166. https://pubs.geoscienceworld.org/gsa/geology/article/25/2/163/206584/Rapid-and-widespread-dispersal-of-flood-sediment

Wheatcroft, R. A., Borgeld, J. C., Born, R. S., Drake, D. E., Leithold, E. L., Nittrouer, Charles, A., & Sommerfield, C. K. (1996). The Anatomy of an Oceanic Flood Deposit. *Oceanography*, *9*(3), 158–162. https://www.jstor.org/stable/43924766

Wheatcroft, R. A. (2006). Time-series measurements of macrobenthos abundance and sediment bioturbation intensity on a flood-dominated shelf. Progress in Oceanography, 71(1), 88–122. https://doi.org/10.1016/j.pocean.2006.06.002

Wheatcroft, R. A., Stevens, A. W., Hunt, L. M., & Milligan, T. G. (2006). The large-scale distribution and internal geometry of the fall 2000 Po River flood deposit: Evidence from digital X-radiography. *Continental Shelf Research*, *26*(4), 499–516. https://doi.org/10.1016/j.csr.2006.01.002

Wright, L. D. (1977). Sediment transport and deposition at river mouths: A synthesis. *Bulletin of the Geological Society of America*, *88*(6), 857–868. https://doi.org/10.1130/0016-7606(1977)88<857:STADAR>2.0.CO;2

Winchester, P. D. (1971). Geology of the Freeport Rocks [Rice University]. https://scholarship.rice.edu/bitstream/handle/1911/89963/RICE0998.pdf?sequence=1

Yang, Y., Chen, F., Zhang, L., Liu, J., Wu, S., & Kang, M. (2012). Comprehensive Assessment of Heavy Metal Contamination in Sediment of the Pearl River Estuary and Adjacent Shelf. *Marine Pollution Bulletin*, *64*(9), 1947–1955. https://doi.org/10.1016/j.marpolbul.2012.04.024

APPENDIX

September 10, 2017

Site	Lat	Long	Harvey(cm)	Sand(%)	Silt(%)	Clay(%)
Bra-04	28.7519	-95.41	12	19.41	47.27	33.32
Bra-05	28.7891	-95.402	10	7.76	52.64	39.59
Bra-06	28.8232	-95.397	3	18.97	47.46	33.56
Bra-07	28.8394	-95.391	4	1	62.2	36.79
Bra-08	28.8584	-95.388	3	6.35	57.61	36.04
D5-06	28.7563	-95.52	0	0	0	0
D4-06	28.7776	-95.478	0	0	0	0
D3-06	28.7999	-95.438	4	18.81	55.53	25.65
S-04	28.8439	-95.36	12	1.79	53.21	45
U1-06	28.8515	-95.32	4.5	23.89	48.56	27.54
U2-06	28.8746	-95.293	0	0	0	0

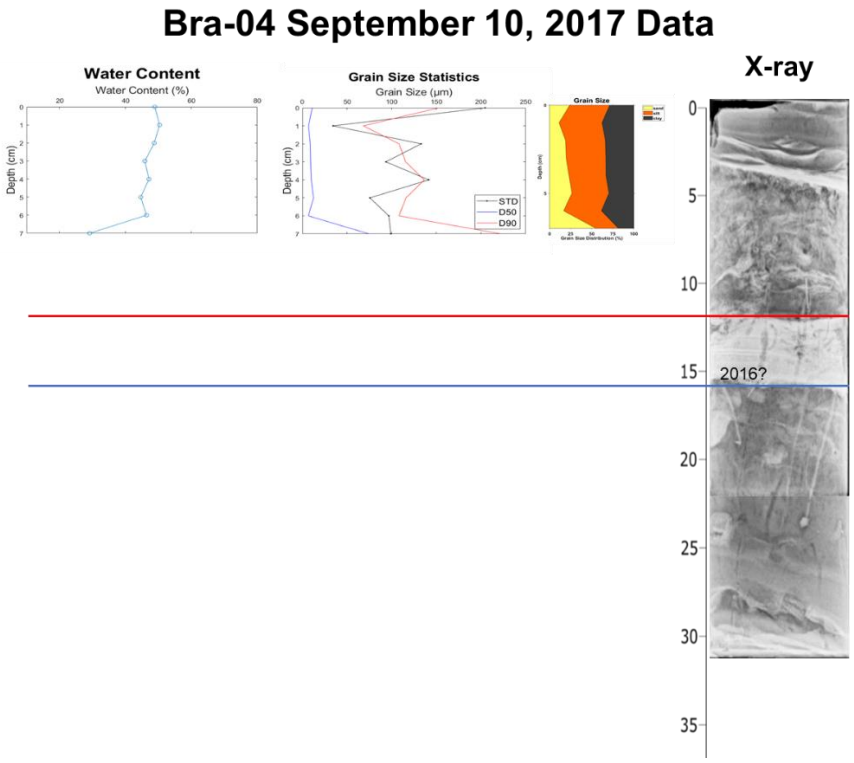

Bra-05: September 10, 2017 Data

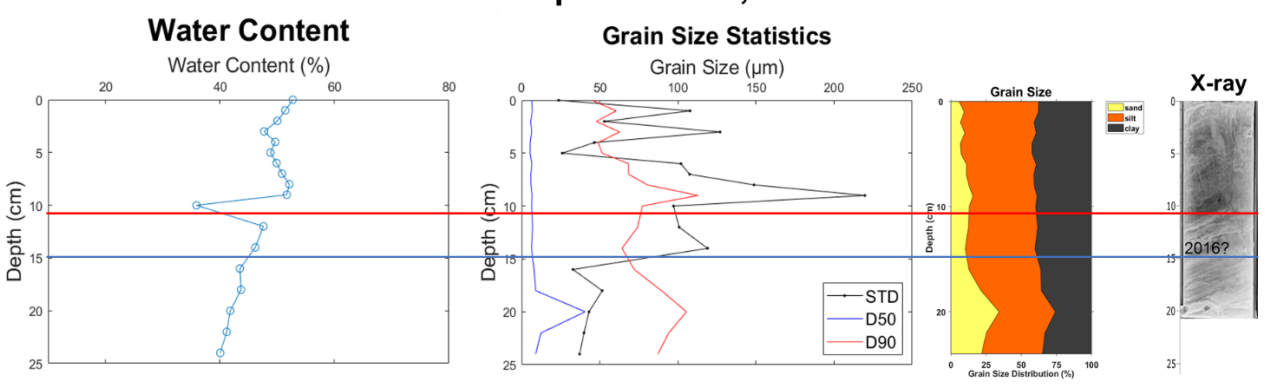

Bra-06: September 10, 2017 Data

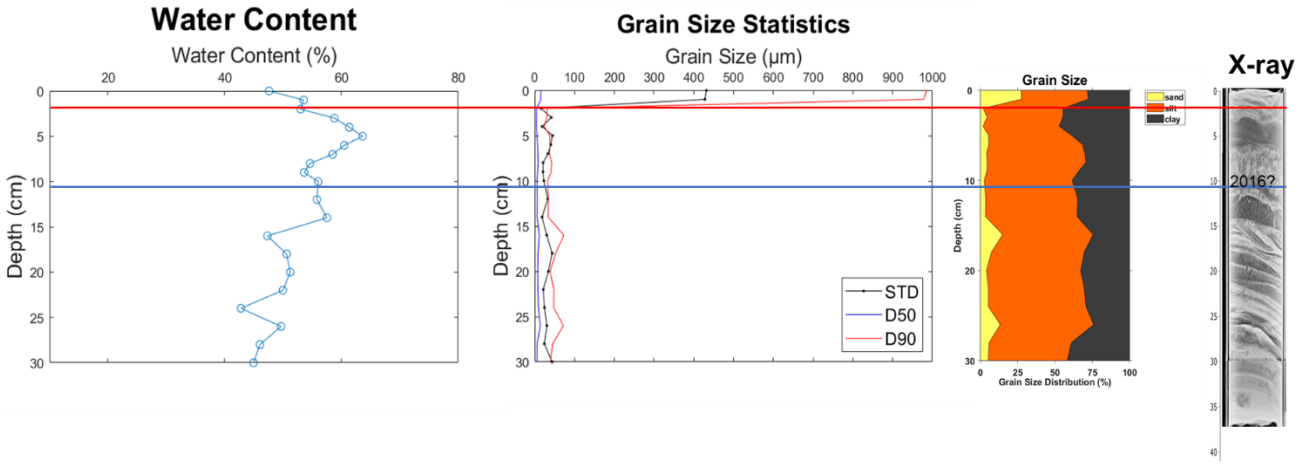

Bra-07: September 10, 2017 Data

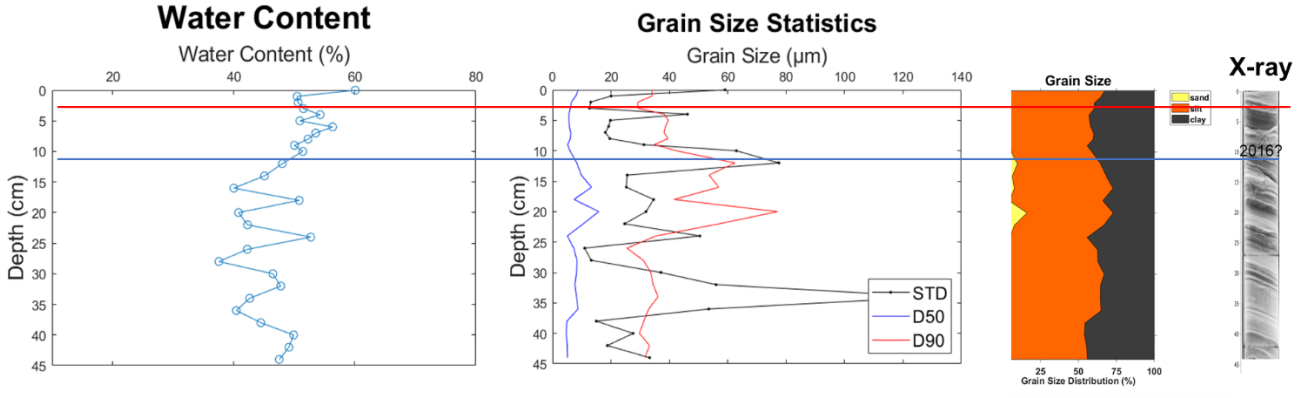

Bra-08: September 10, 2017 Data

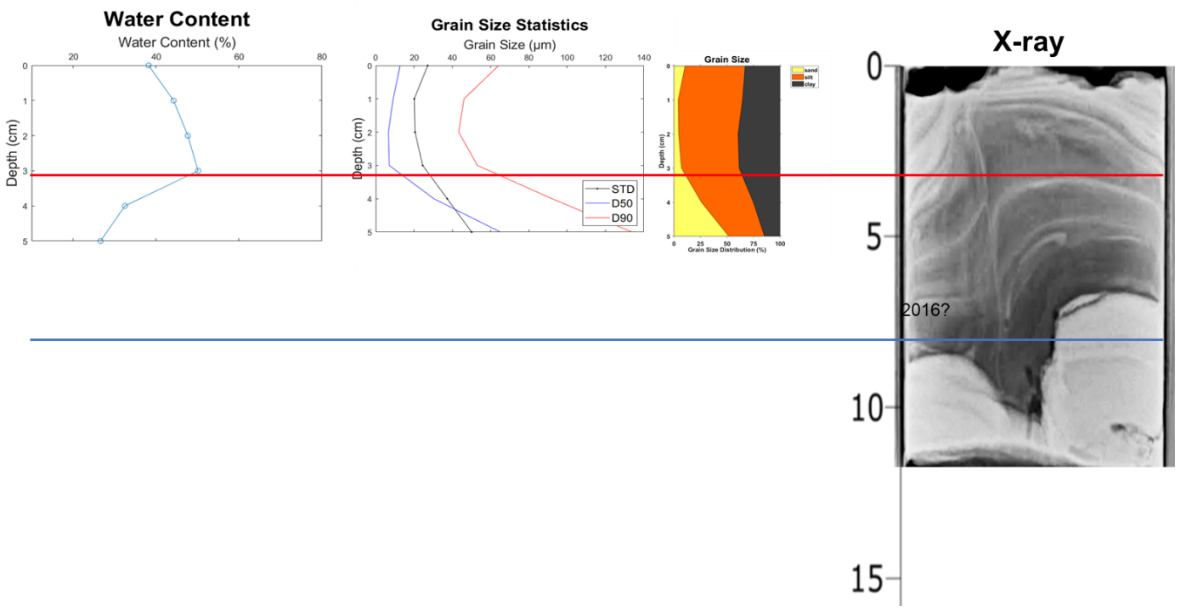

D5-06: September 10, 2017 Data

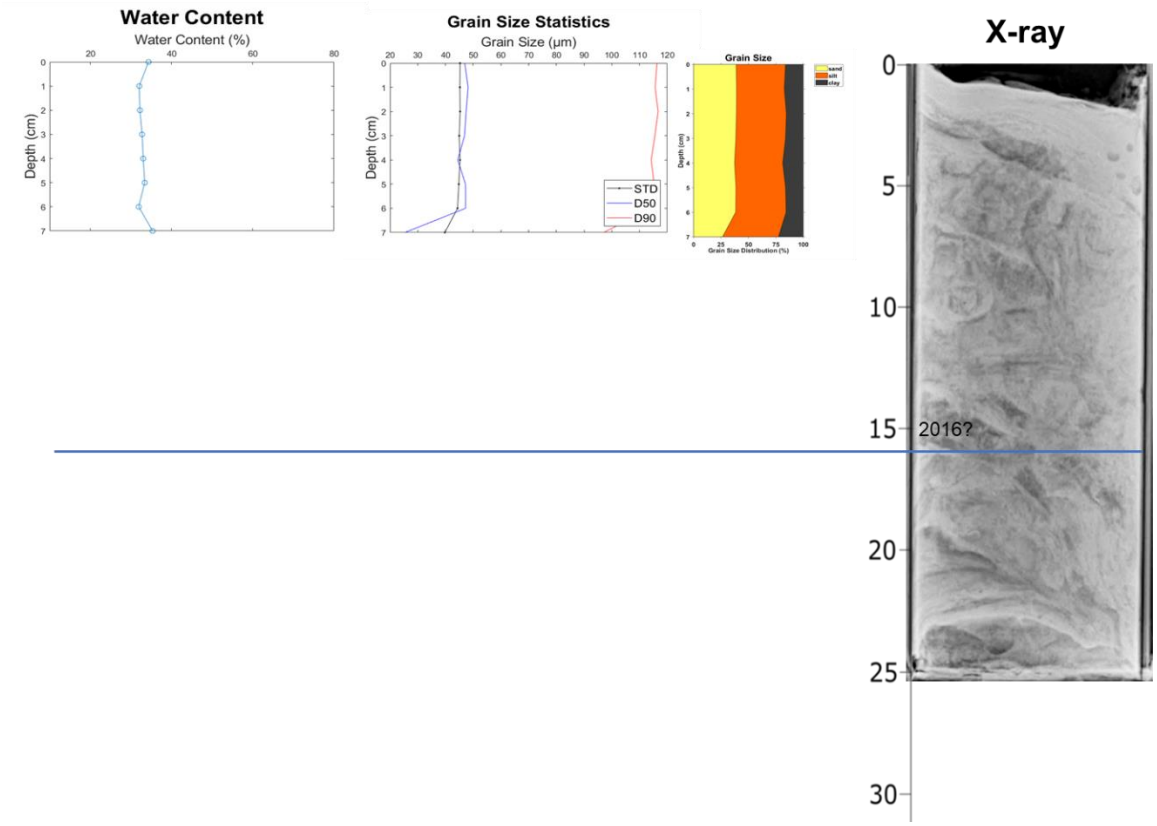

D4-06: September 10, 2017 Data

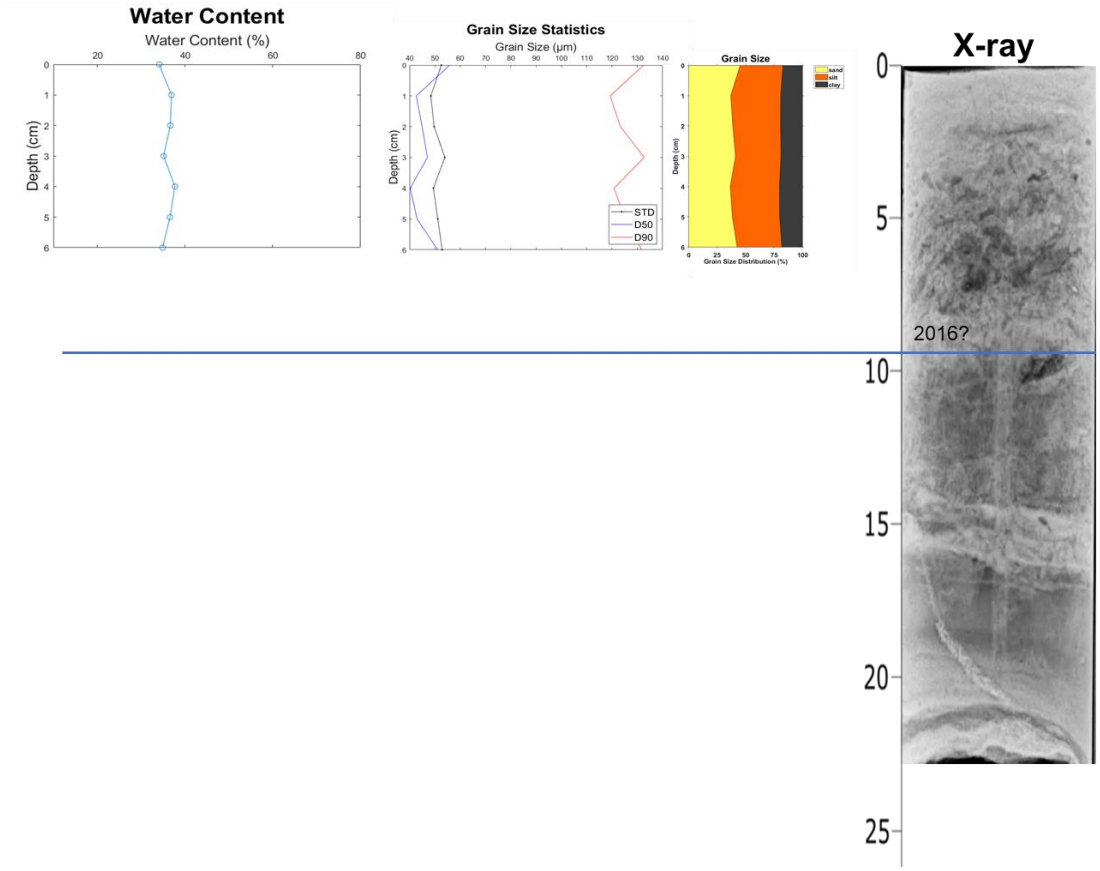

D3-06: September 10, 2017 Data

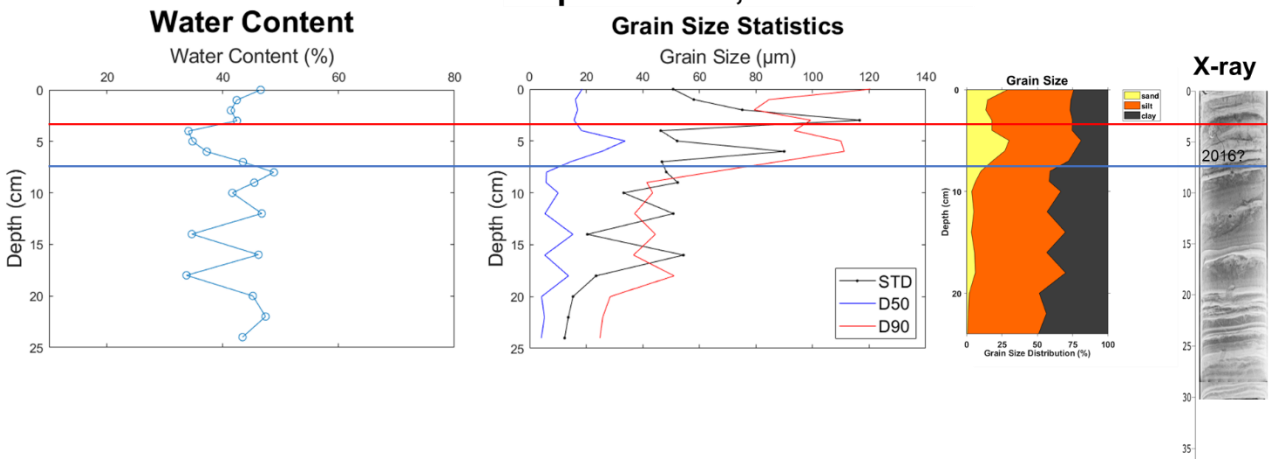

S-04: September 10, 2017 Data

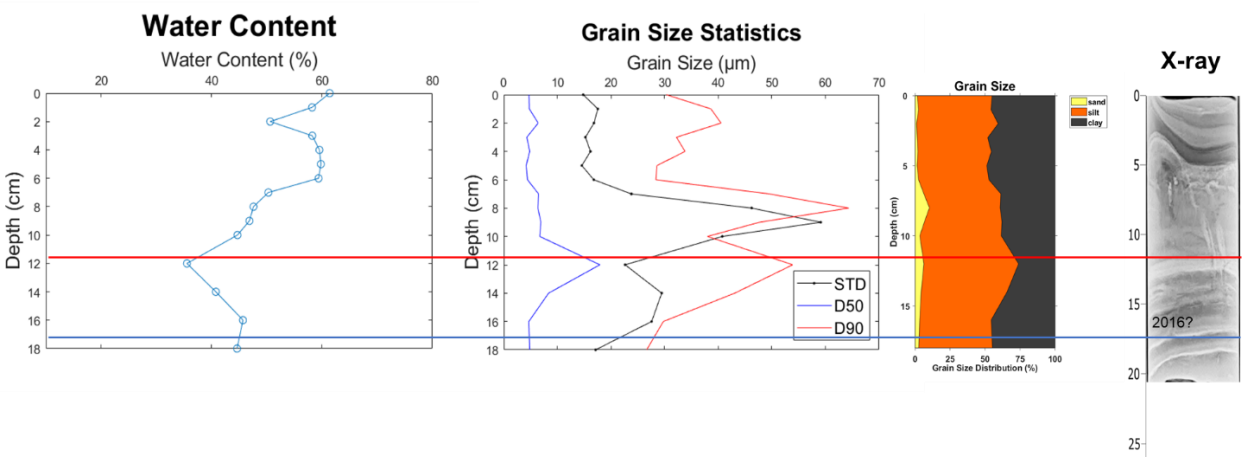

U2-06: September 10, 2017 Data

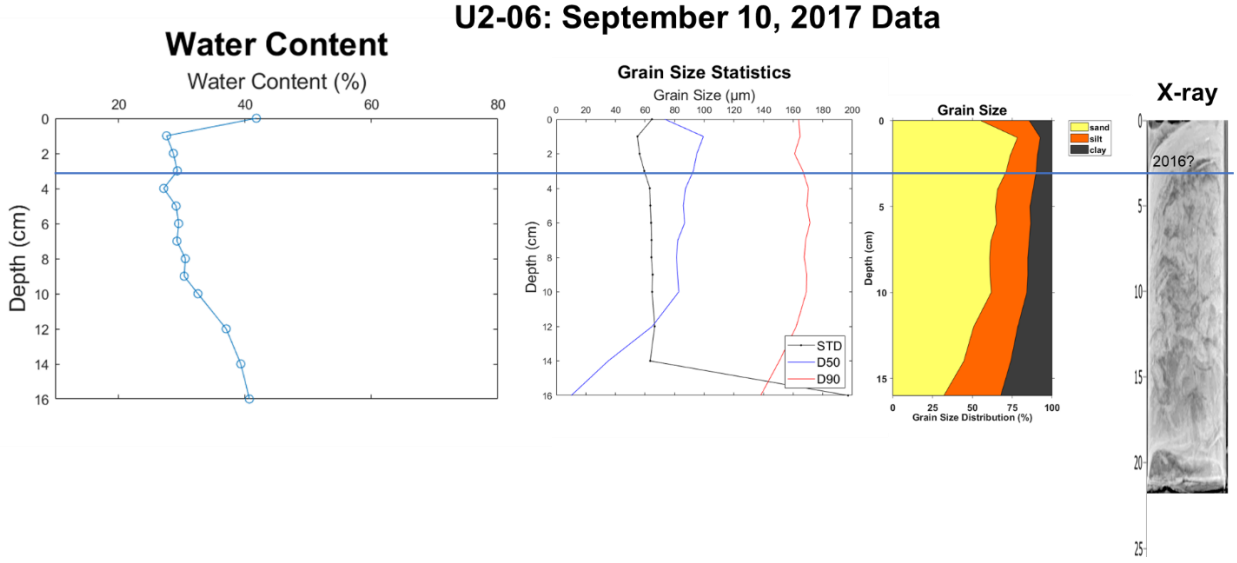

October 29, 2017

Site	Lat	Long	Harvey(cm)	Sand(%)	Silt(%)	Clay(%)
D2-06	28.8072	-95.404	4.5	2.9	53.5	43.6
D2-08	28.7912	-95.392	8.5	3.98	51.39	44.63
D2-12	28.7639	-95.372	0	0	0	0
D3-06	28.799	-95.434	6	10.36	63.11	26.54
D3-08	28.7816	-95.418	3.5	27.14	48.9	23.96
D3-12	28.7537	-95.4	11	13.68	61.24	25.07
D4-06	28.778	-95.477	0	0	0	0
D4-08	28.7574	-95.464	0	0	0	0
D4-12	28.7321	-95.446	0	0	0	0
D5-06	28.7553	-95.521	0	0	0	0
D5-08	28.7349	-95.504	0	0	0	0
D5-12	28.7128	-95.484	0	0	0	0
J-04	28.8311	-95.386	8	7.4	51.47	41.13
J-06	28.8161	-95.375	4	6.02	55.75	38.23
J-08	28.8003	-95.36	6	7.03	58.05	34.92
J-12	28.7748	-95.343	4	13.31	59.89	26.8
S-04	28.8454	-95.358	2.5	2.87	61.01	36.12
S-06	28.8296	-95.348	4	9.31	62.08	28.61
S-08	28.8147	-95.338	12	4.94	60.61	34.44
S-12	28.7836	-95.317	6	8.8	66.9	24.3
U1-06	28.8525	-95.318	6	37.15	42.57	20.28
U1-08	28.8375	-95.306	4	4.92	57.2	37.88
U1-12	28.8072	-95.284	9	6.23	69.57	24.2
U2-06	28.8711	-95.292	0	0	0	0
U2-08	28.8593	-95.282	9	9.54	59.62	30.84
U2-12	28.8289	-95.254	6	15.78	59.56	24.66

D2-06: October 29, 2017 Data

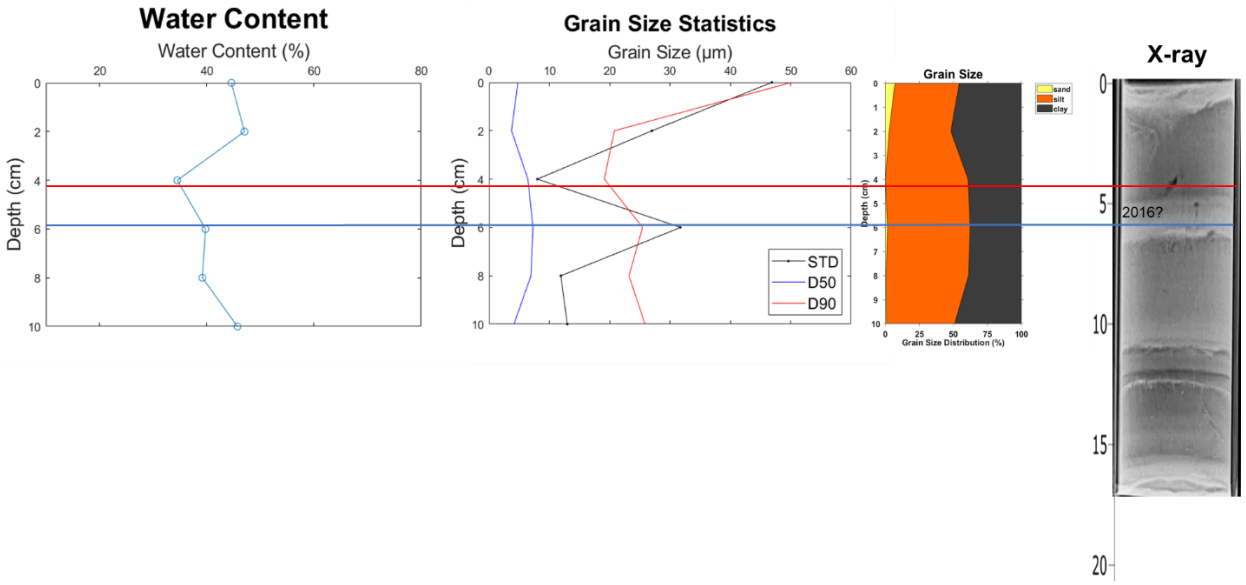

D2-08: October 29,2017 Data

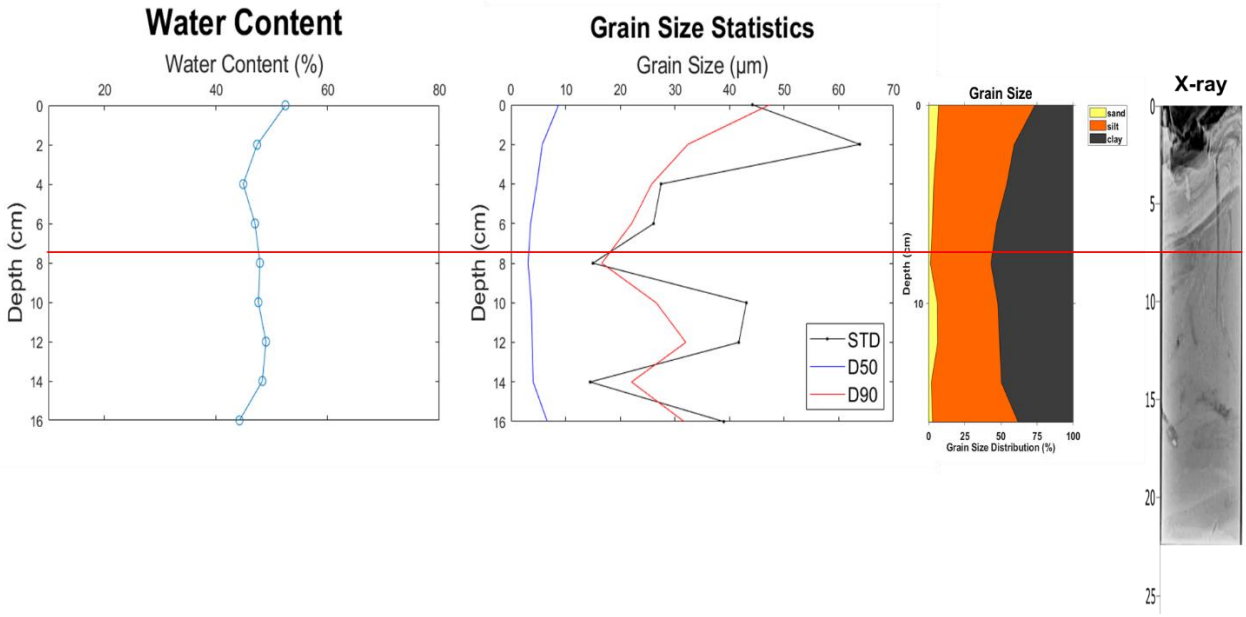

D3-06: October 29, 2017 Data

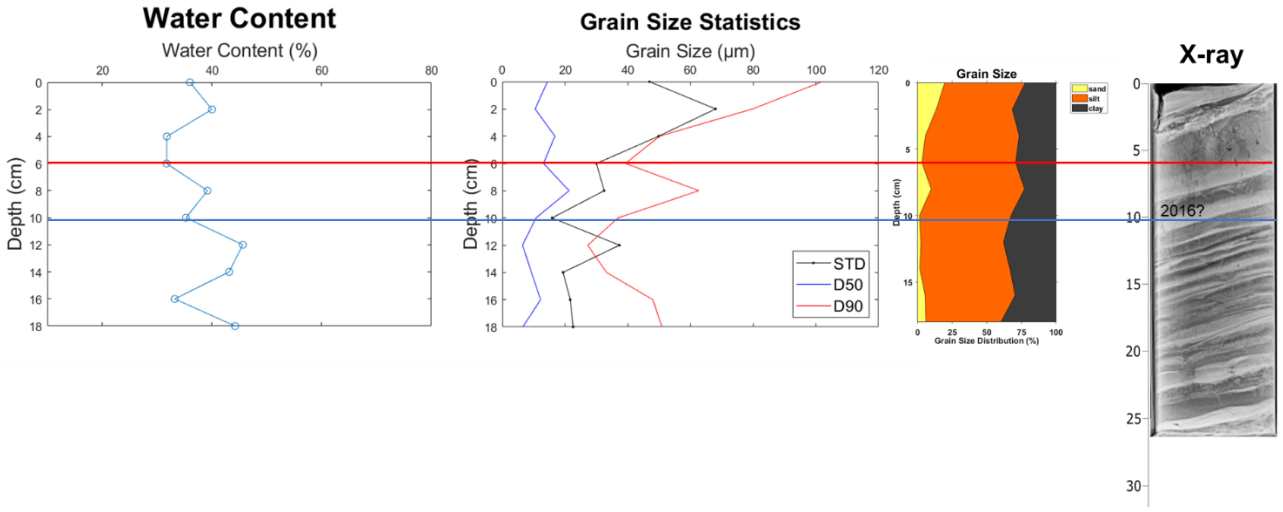

D3-08: October 29, 2017 Data

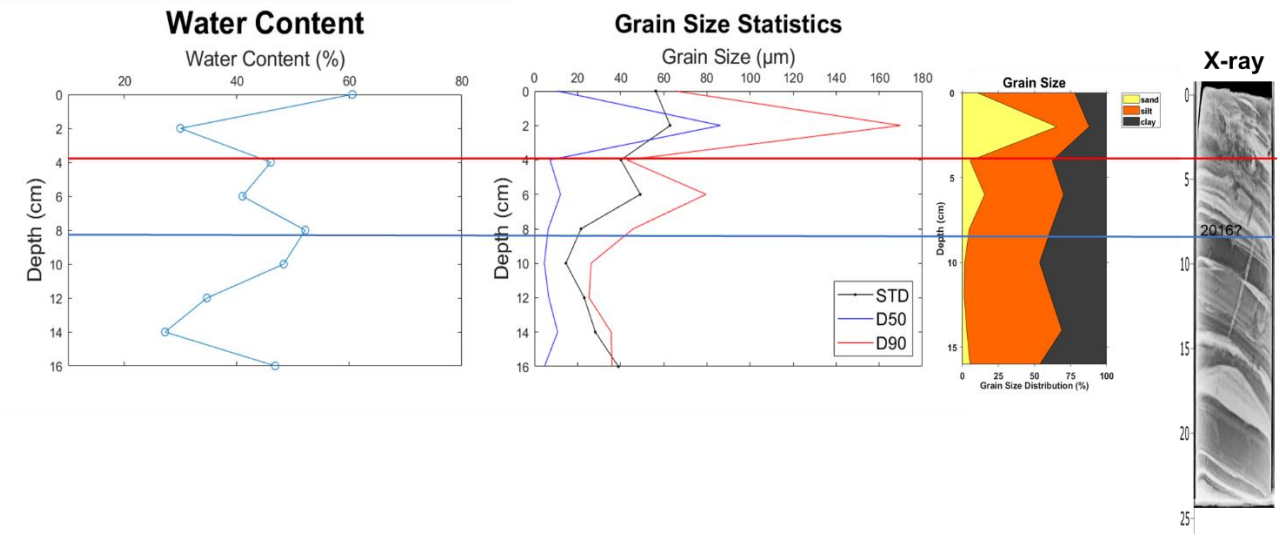

D3-12: October 29, 2017 Data

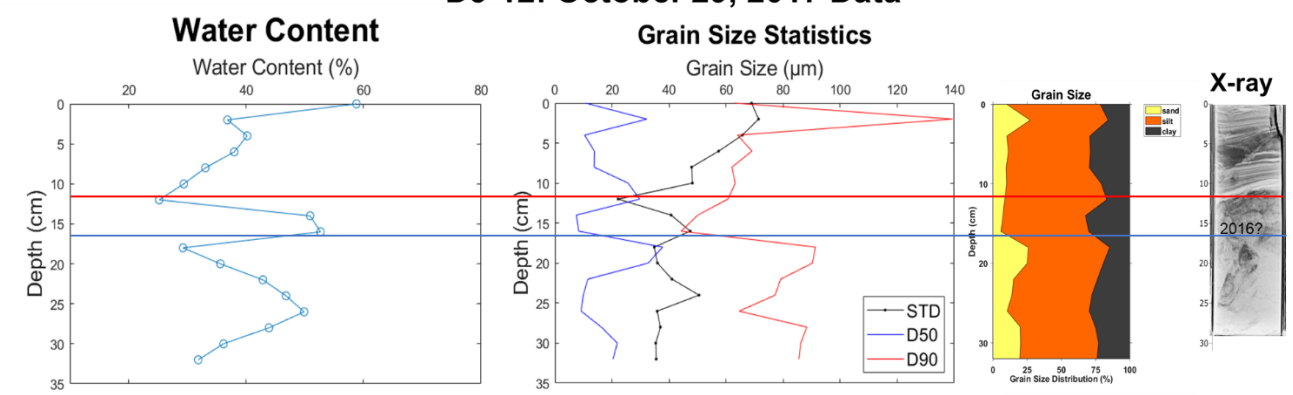

D4-08: October 29, 2017 Data

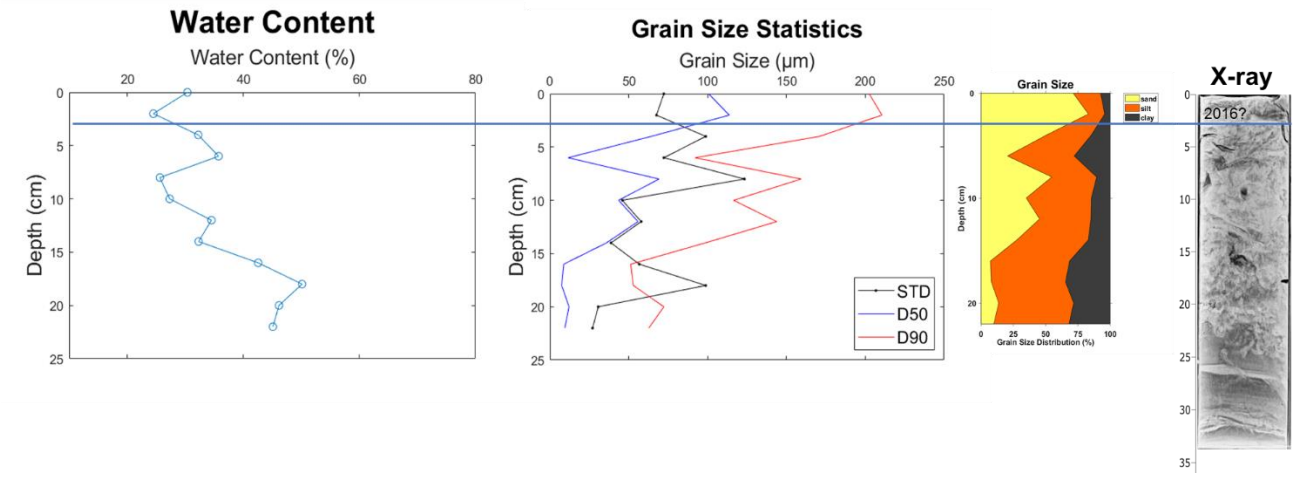

D4-12: October 29, 2017 Data

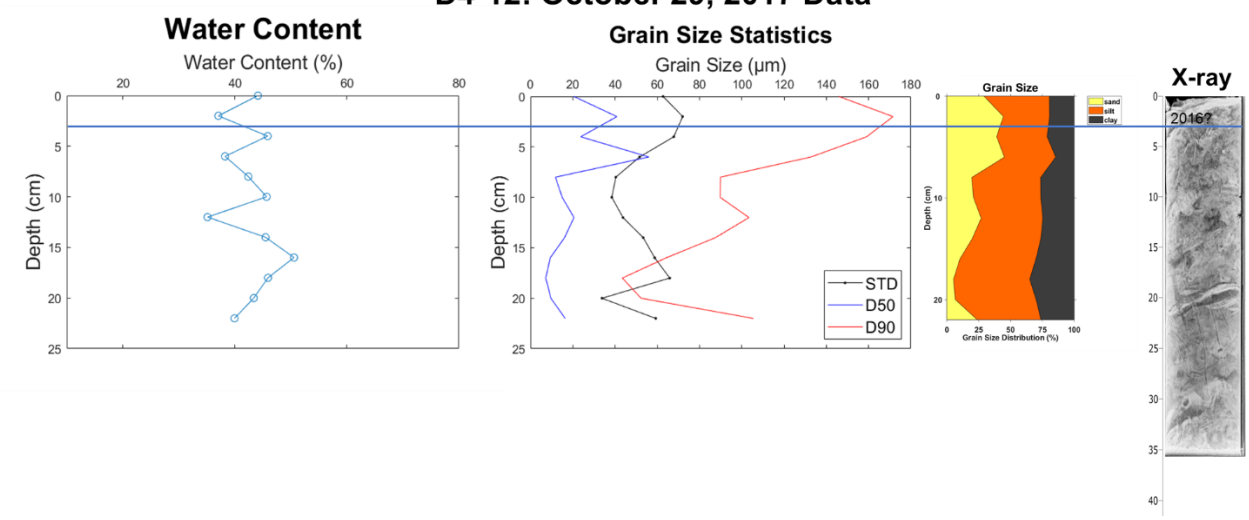

D5-06: October 29, 2017 Data

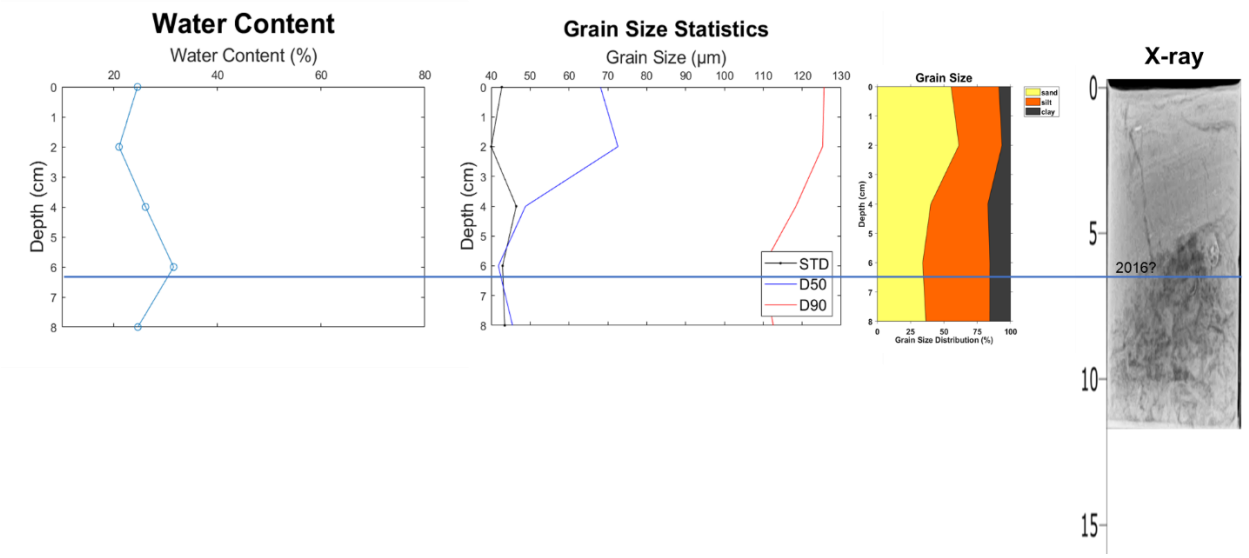

D5-08: October 29, 2017 Data

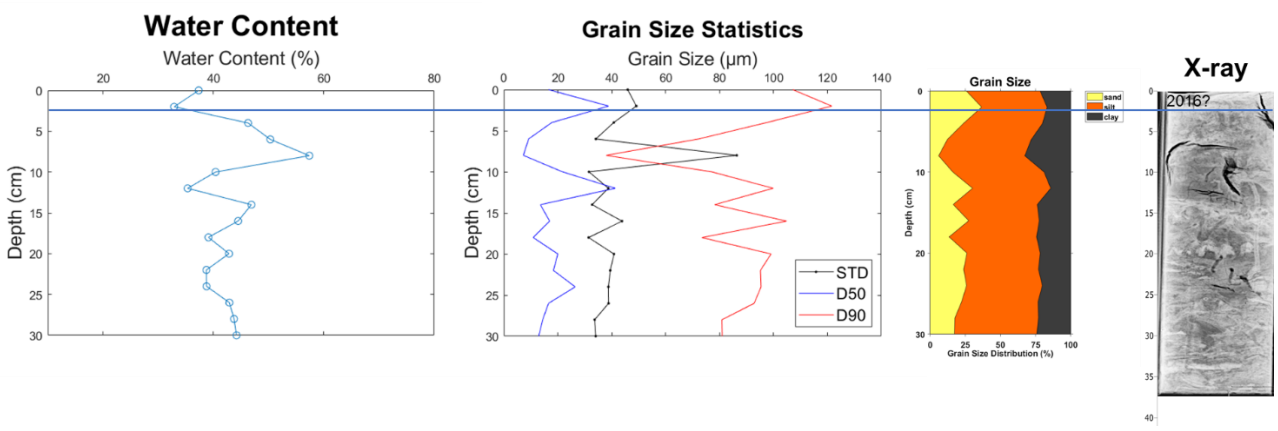

D5-12: October 29, 2017 Data

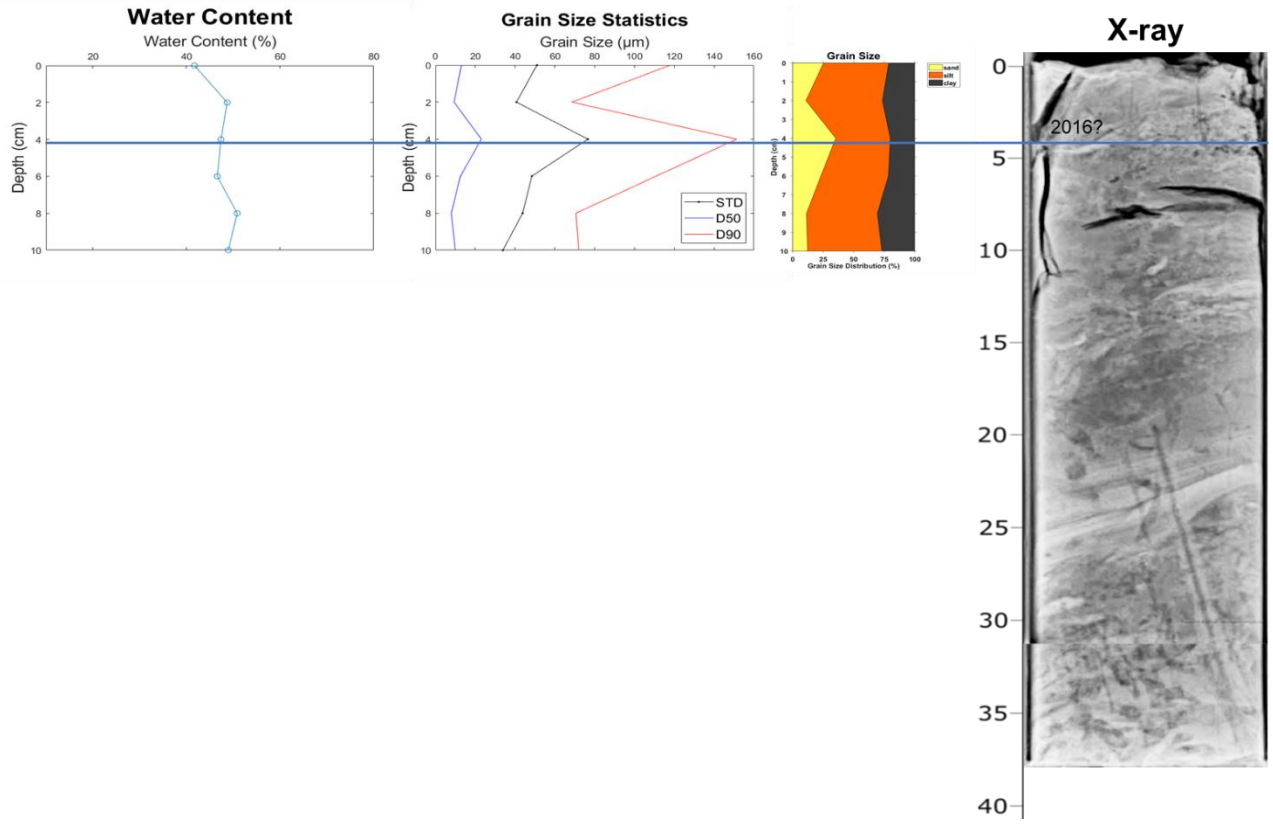

J-04: October 29, 2017 Data

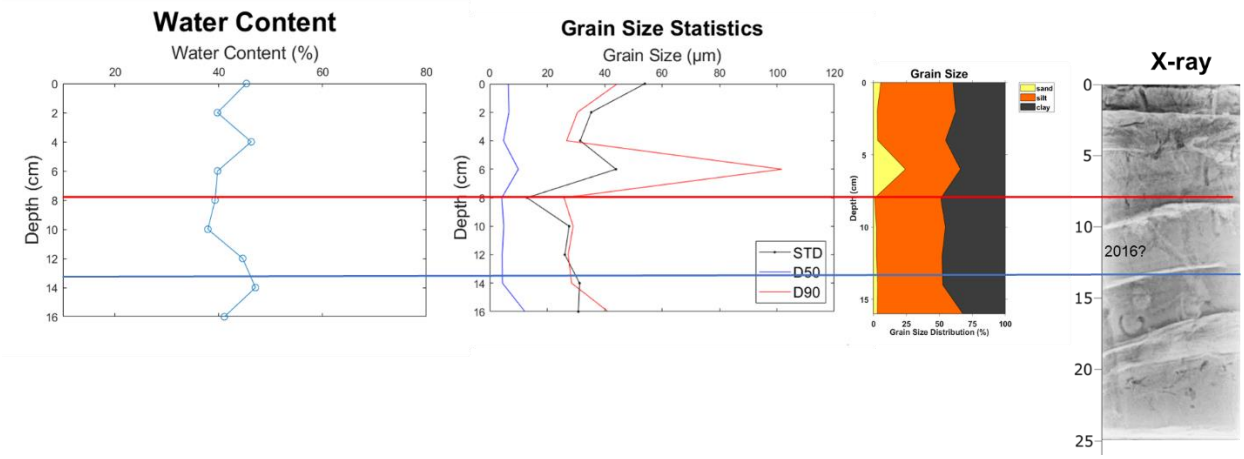

J-06: October 29, 2017 Data

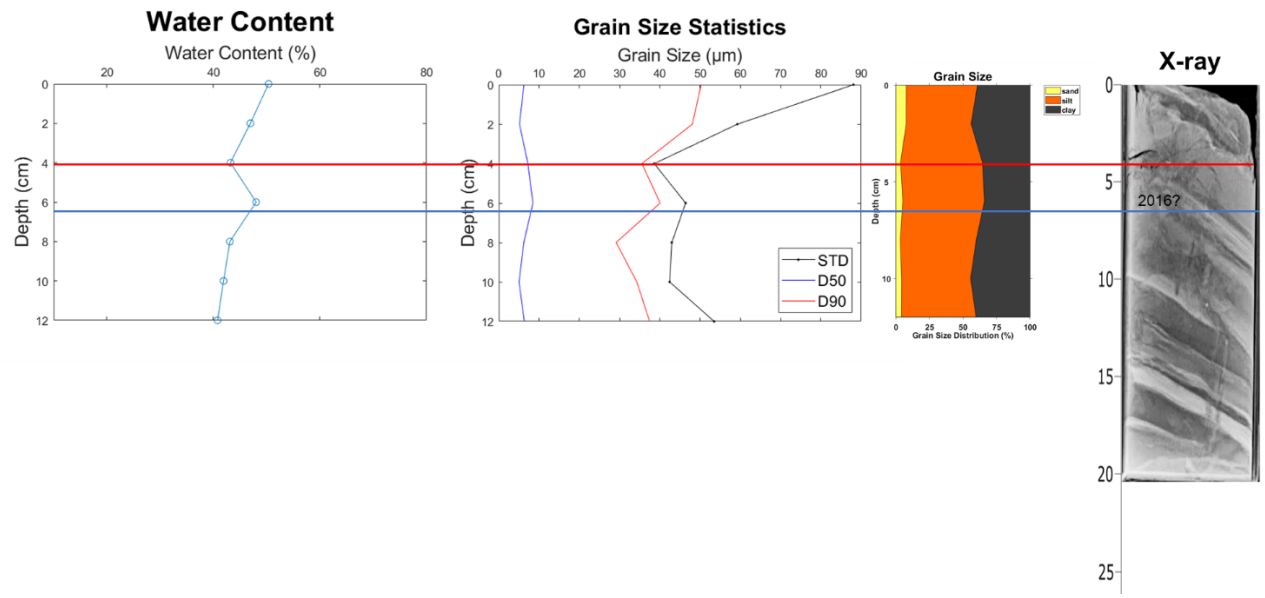

J-08: October 29, 2017 Data

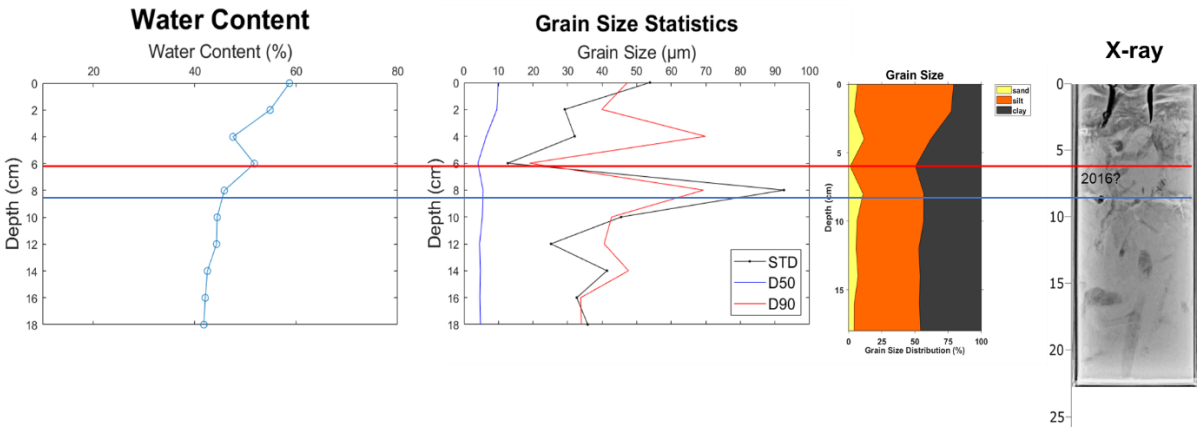

J-12: October 29, 2017 Data

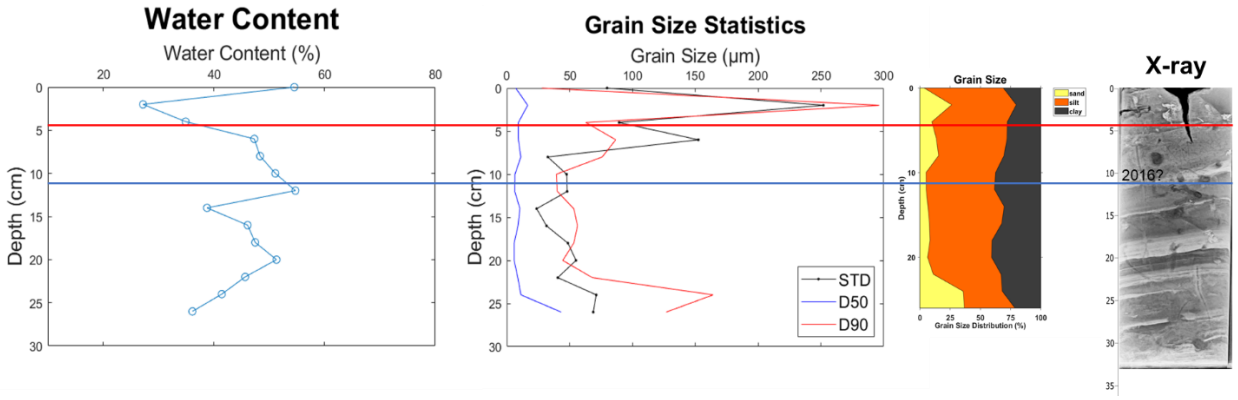

S-04: October 29, 2017 Data

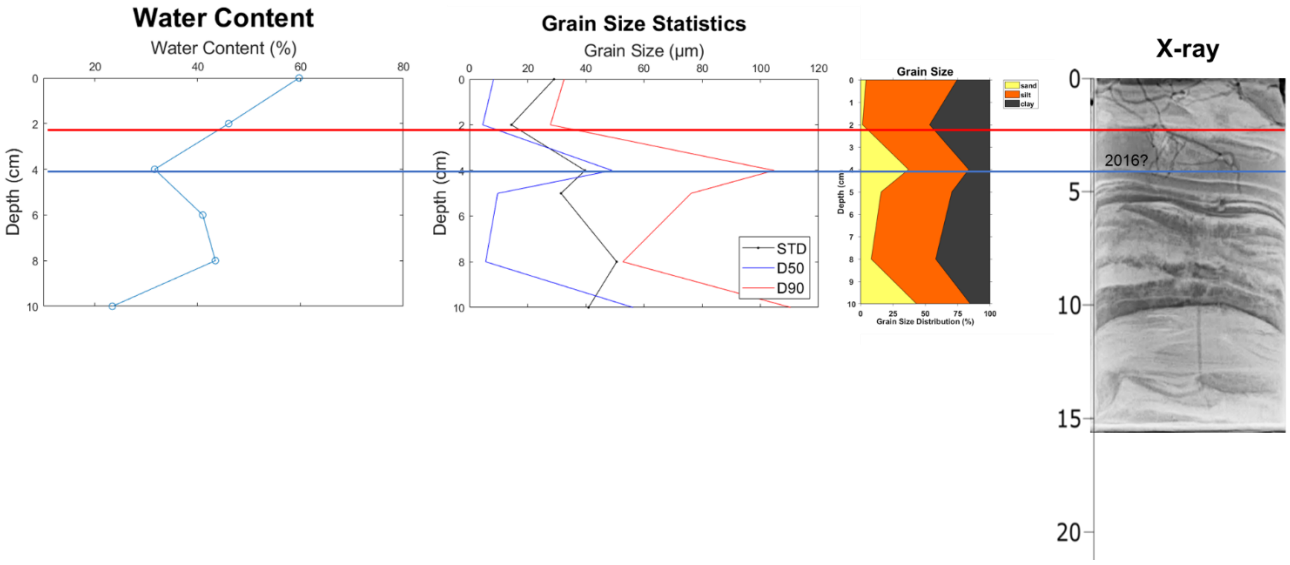

S-06: October 29, 2017 Data

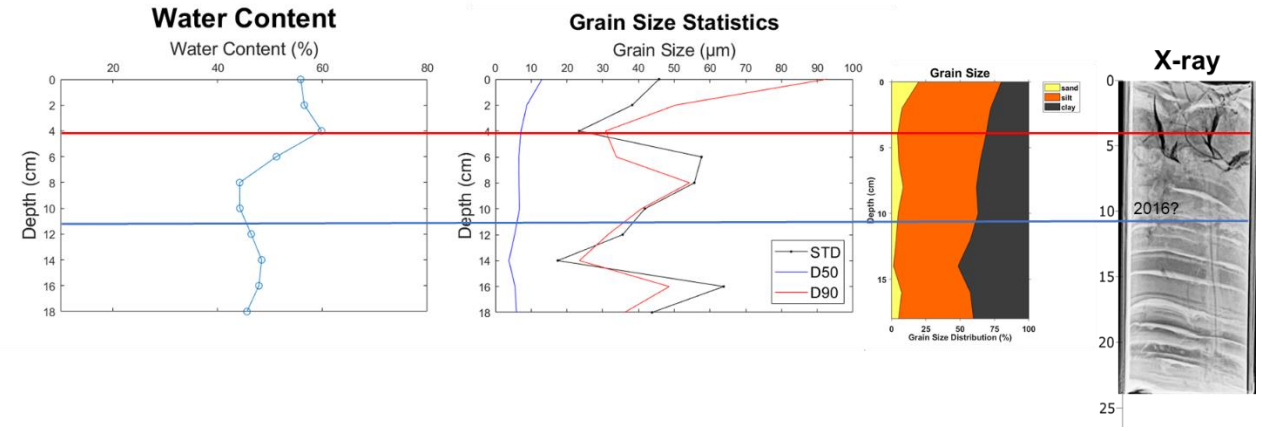

S-08: October 29, 2017 Data

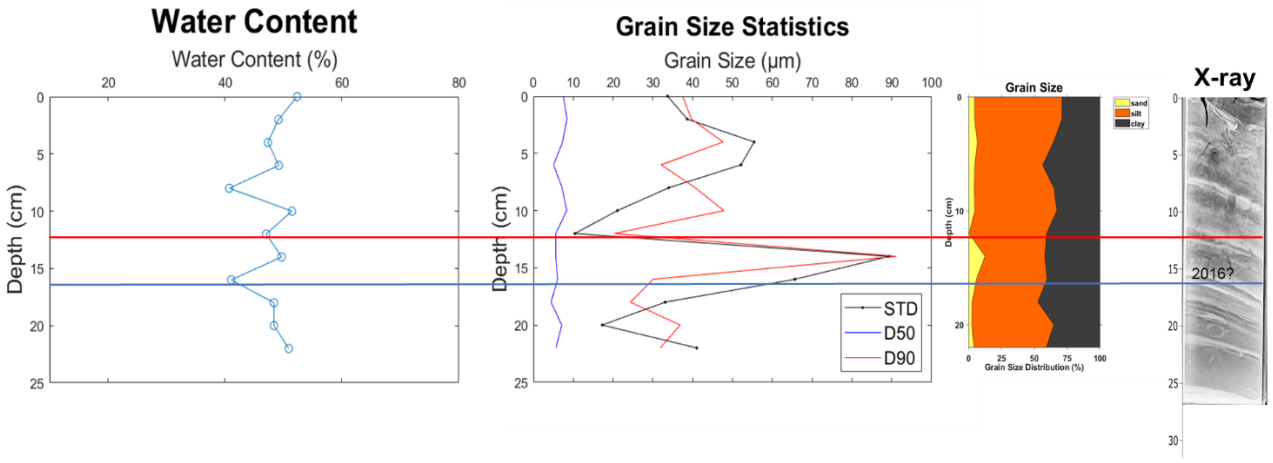

S-12: October 29, 2017 Data

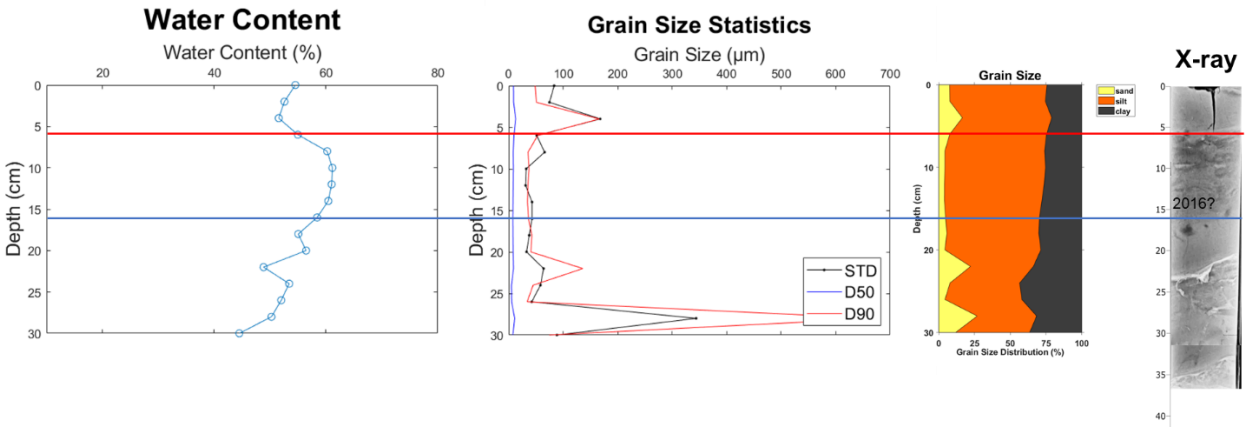

U1-06: October 29, 2017 Data

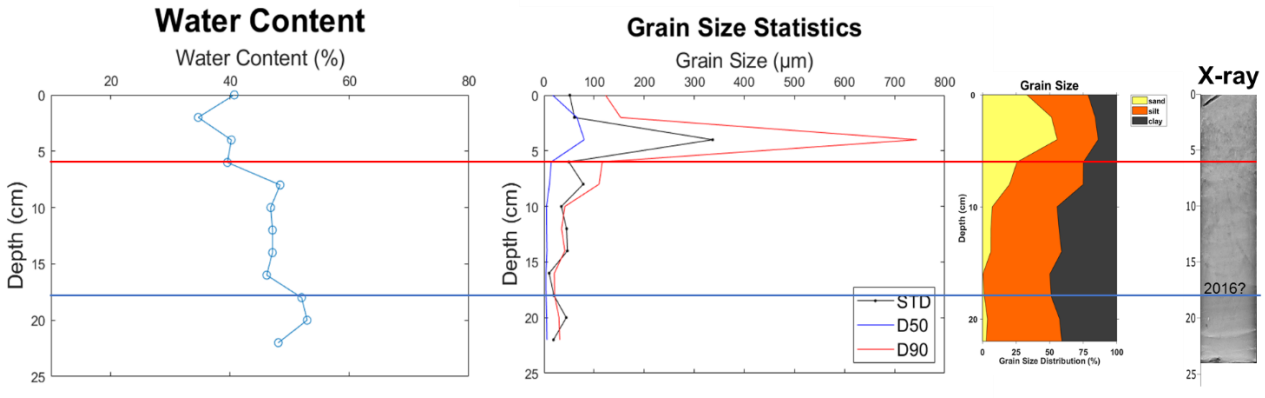

U1-08: October 29, 2017 Data

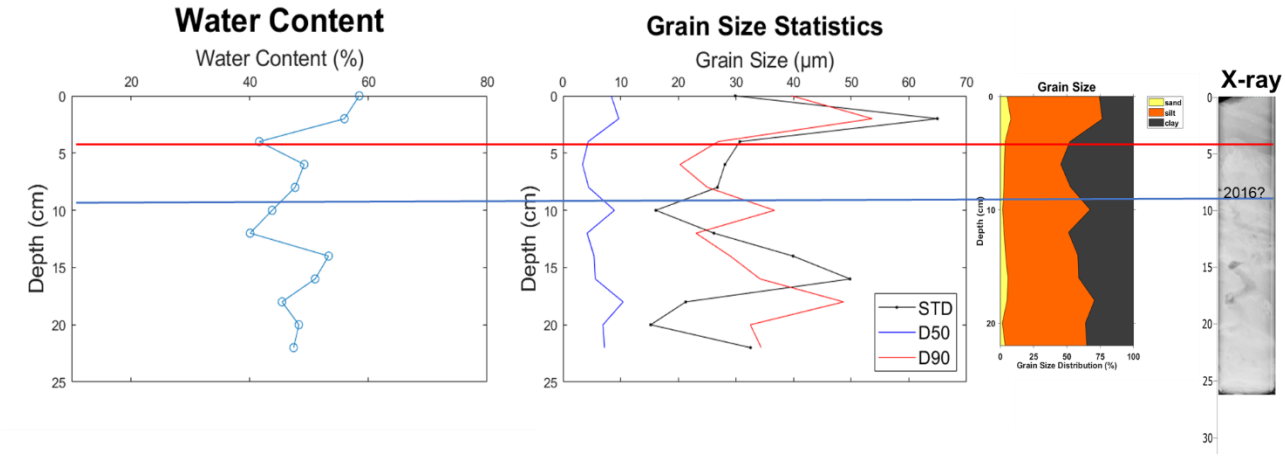

U1-12: October 29, 2017 Data

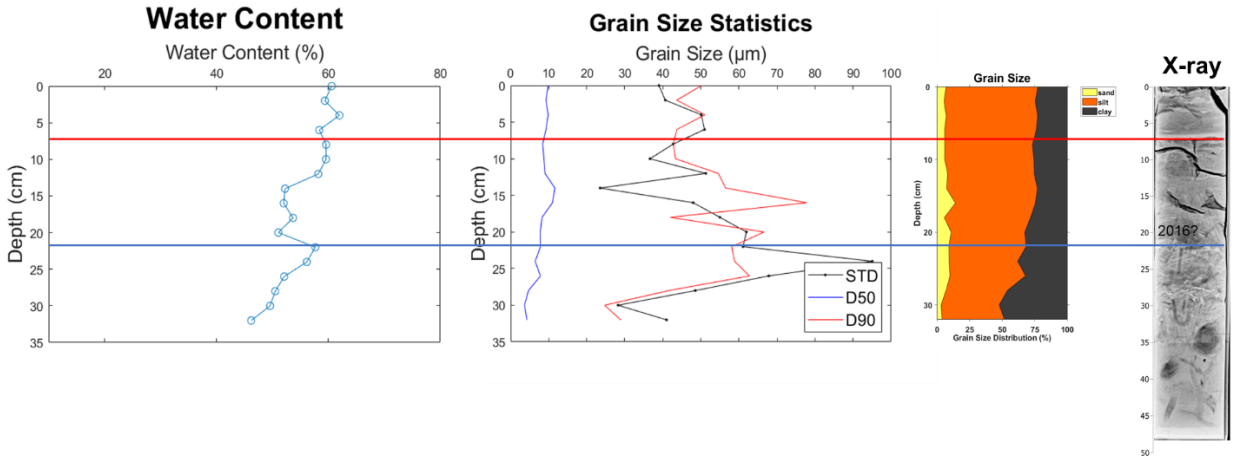

U2-06: October 29, 2017 Data

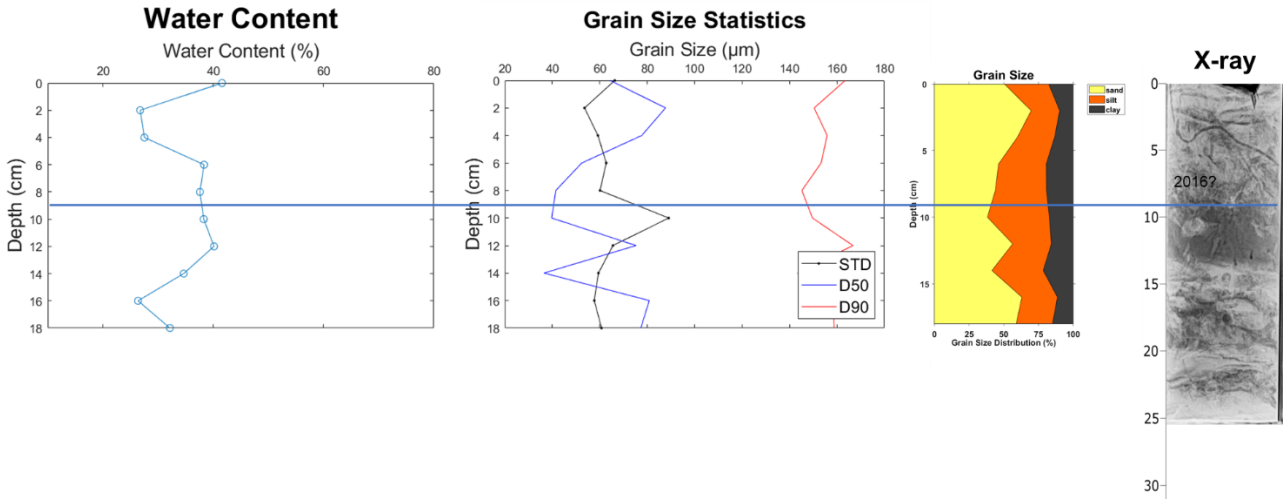

U2-08: October 29, 2017 Data

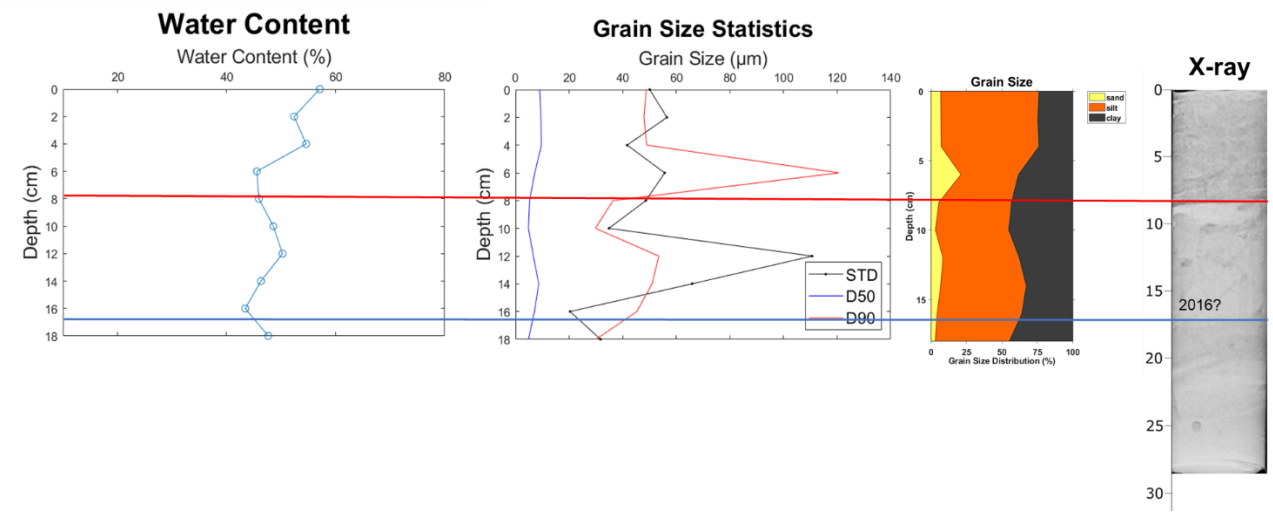

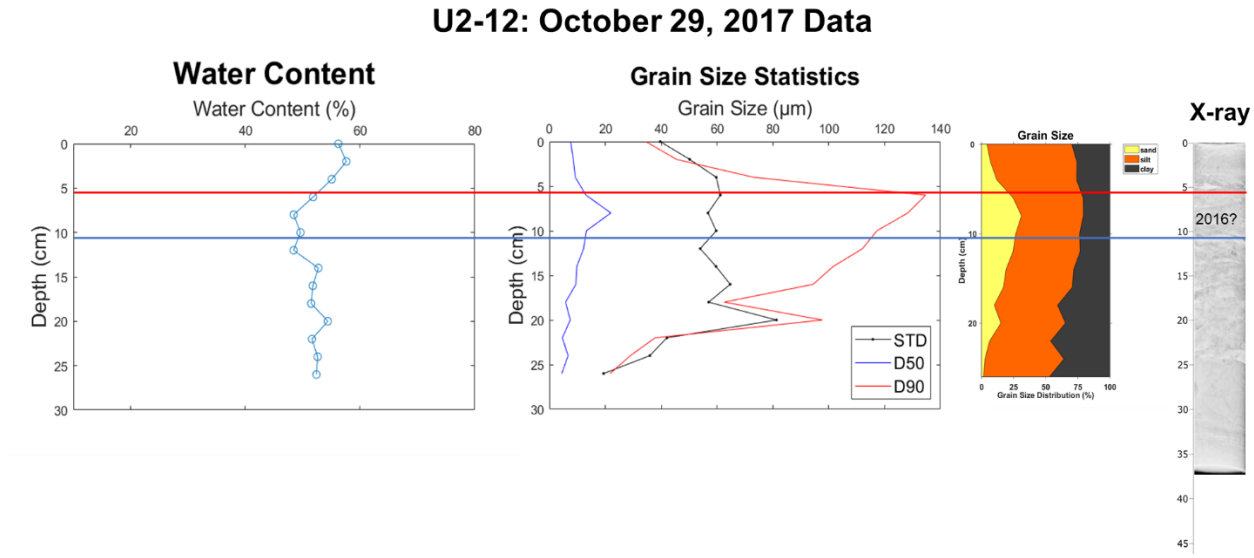
U2-12: October 29, 2017 Data
Water Content
Water Content (%)
Depth (cm)
Grain Size Statistics
Grain Size (µm)
STD
D50
D90
Grain Size
sand
silt
clay
Grain Size Distribution (%)
X-ray
2016?

July 12, 2018

Site	Lat	Long	Harvey(cm)	Sand(%)	Silt(%)	Clay(%)
D2-12	28.7643	-95.372	5	18.21	55.14	26.65
D3-12	28.7541	-95.4	0	0	0	0
D4-12	28.7324	-95.446	0	0	0	0
D5-12	28.7133	-95.483	9	14.92	64.97	20.11
S-12	28.7654	-95.317	0	0	0	0
U1-12	28.8077	-95.284	7	5.37	72.74	21.89
U2-12	28.8298	-95.254	6	5.95	71.24	22.81
X2-1	28.789	-95.271	0	0	0	0
X2-2	28.7773	-95.264	0	0	0	0
X2-3	28.7573	-95.25	0	0	0	0
X3-1	28.7772	-95.307	10	16.01	60.73	23.26
X3-2	28.7606	-95.289	0	0	0	0
X3-3	28.7443	-95.278	0	0	0	0
X4-1	28.7644	-95.358	4	15.91	63.07	21.02
X4-2	28.7529	-95.349	8	8.51	68.38	23.11
X5-1	28.7475	-95.392	0	0	0	0
X5-2	28.7317	-95.368	11	8.23	69.35	22.42
X5-3	28.718	-95.353	0	0	0	0
X5-4	28.7013	-95.332	0	0	0	0
X6-1	28.7245	-95.432	0	0	0	0
X6-2	28.7007	-95.409	0	0	0	0
X6-4	28.6579	-95.364	0	0	0	0
X7-1	28.7179	-95.488	7.5	13.17	64.03	22.81
X7-2	28.6975	-95.465	5.5	17.68	61.24	21.07
X7-3	28.6644	-95.451	3	27.46	53.29	19.25
X7-4	28.6509	-95.391	0	0	0	0
X7-5	28.6392	-95.391	0	0	0	0

D2-12: July 12, 2019 Data

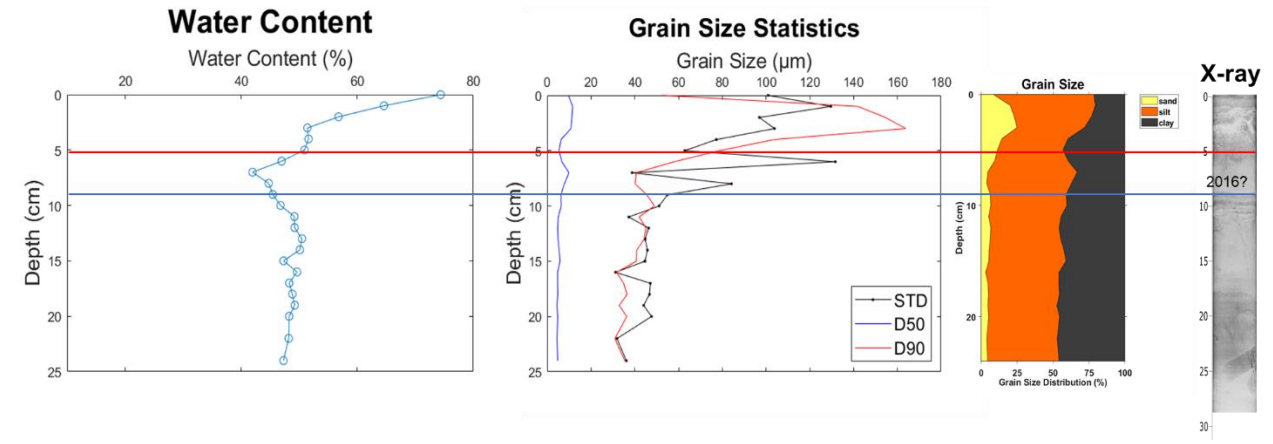

D3-12: July 12, 2018 Data

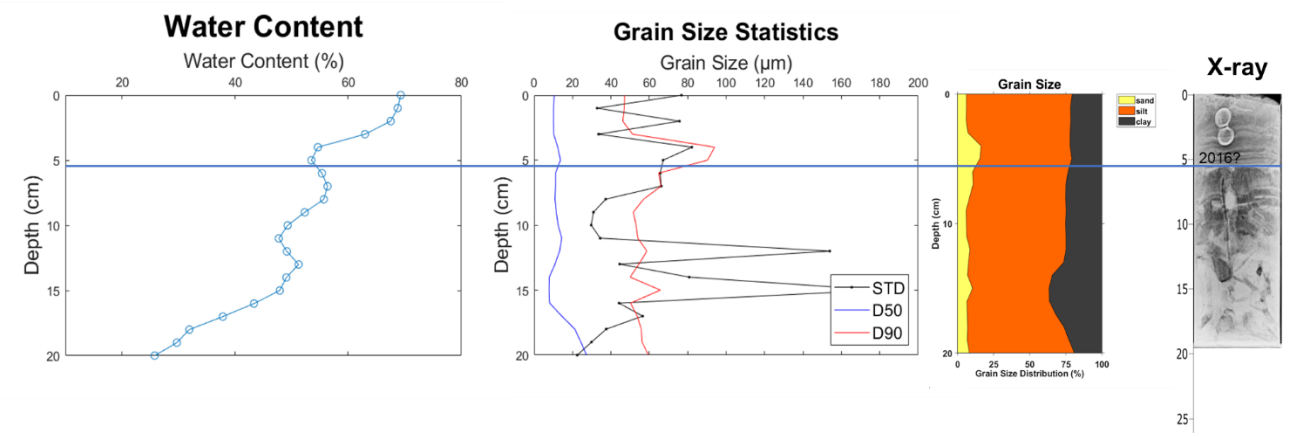

D4-12: July 12, 2018 Data

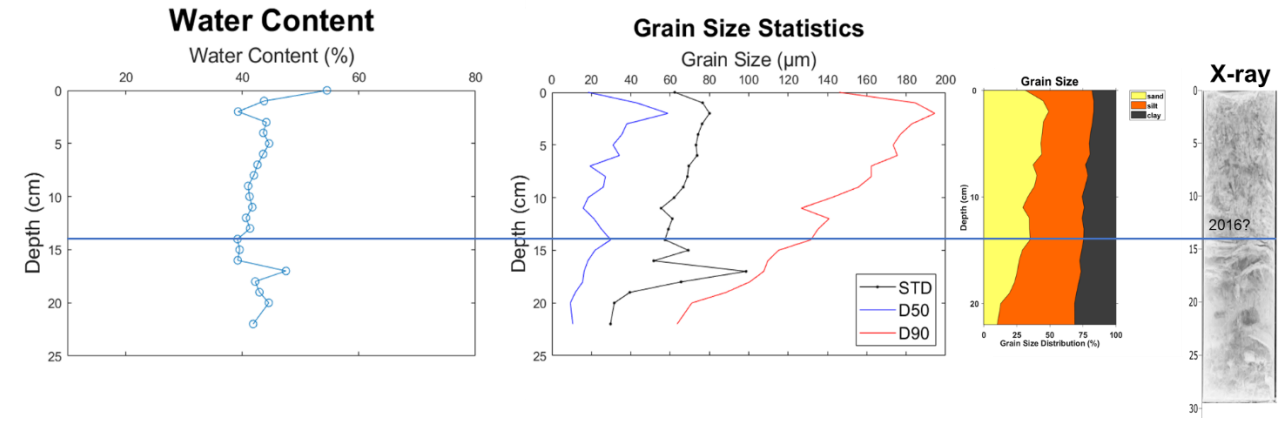

D5-12: July 12, 2018 Data

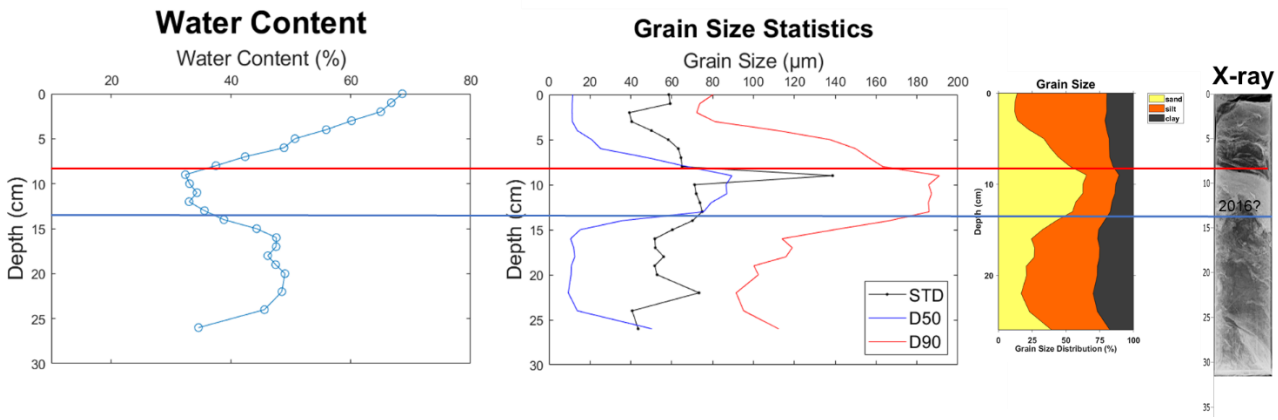

S-12: July 12, 2018 Data

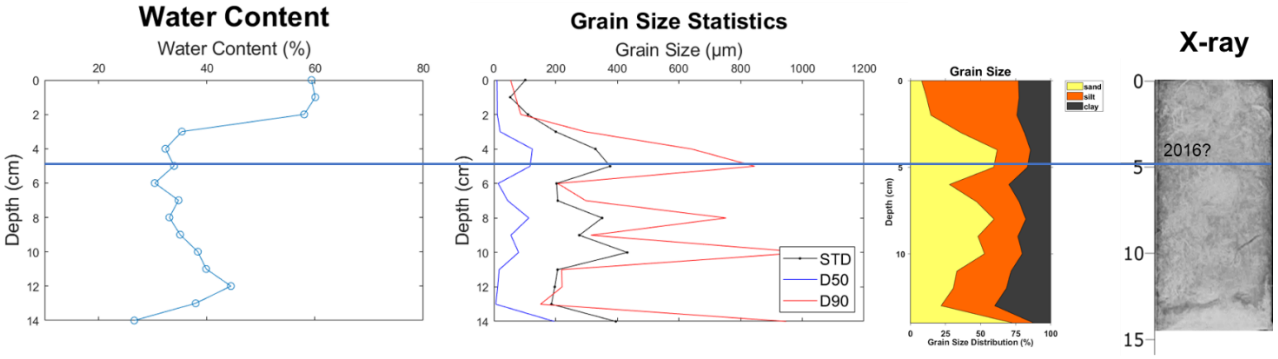

U1-12: July 12, 2018 Data

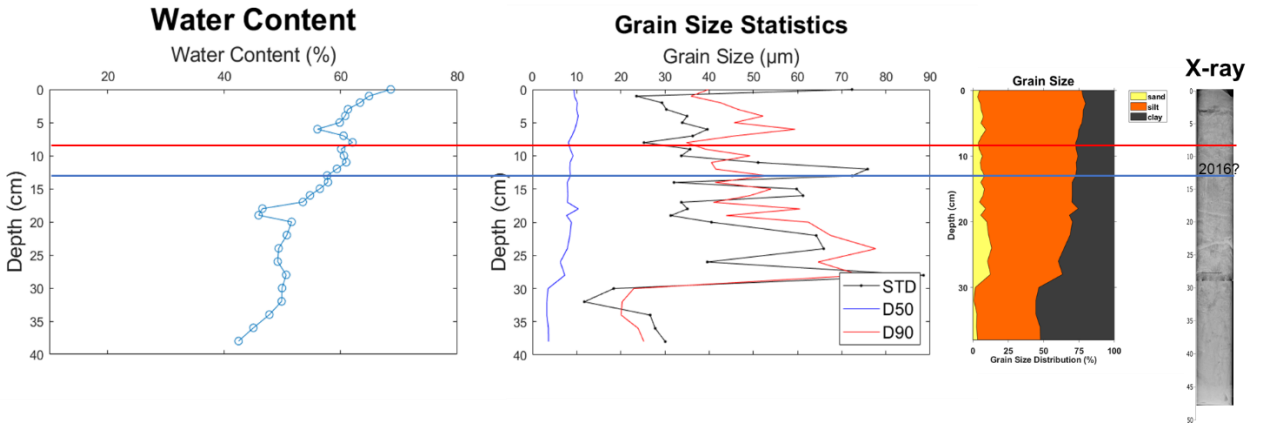

U2-12: July 12, 2018 Data

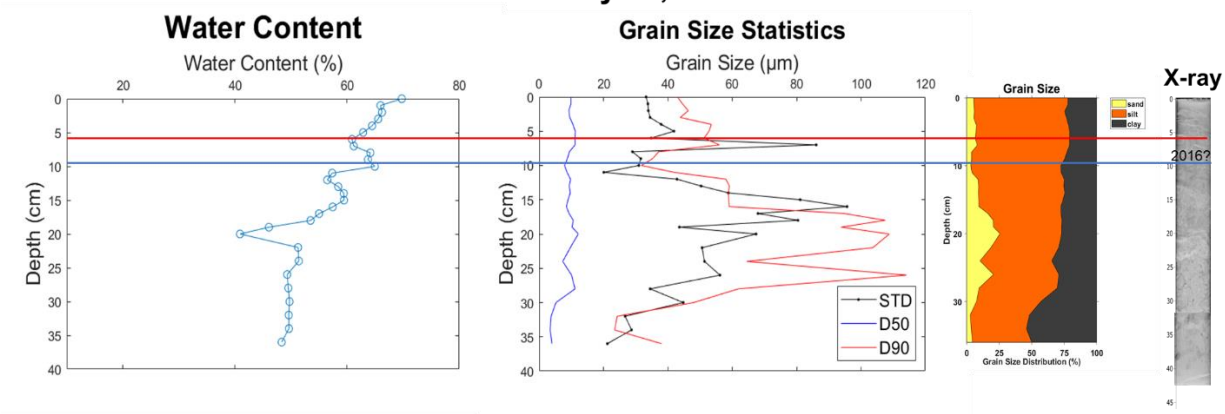

X2-1: July 12, 2018 Data

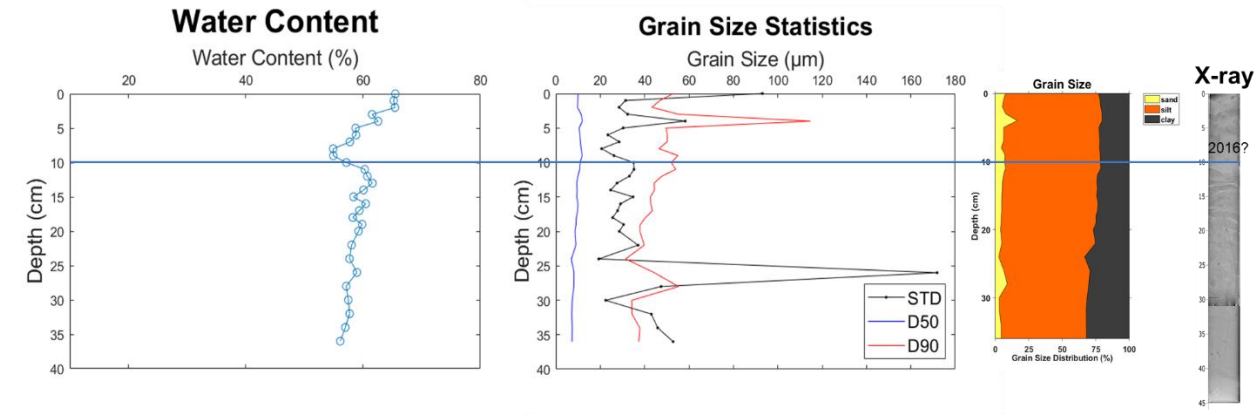

X2-2: July 12, 2018 Data

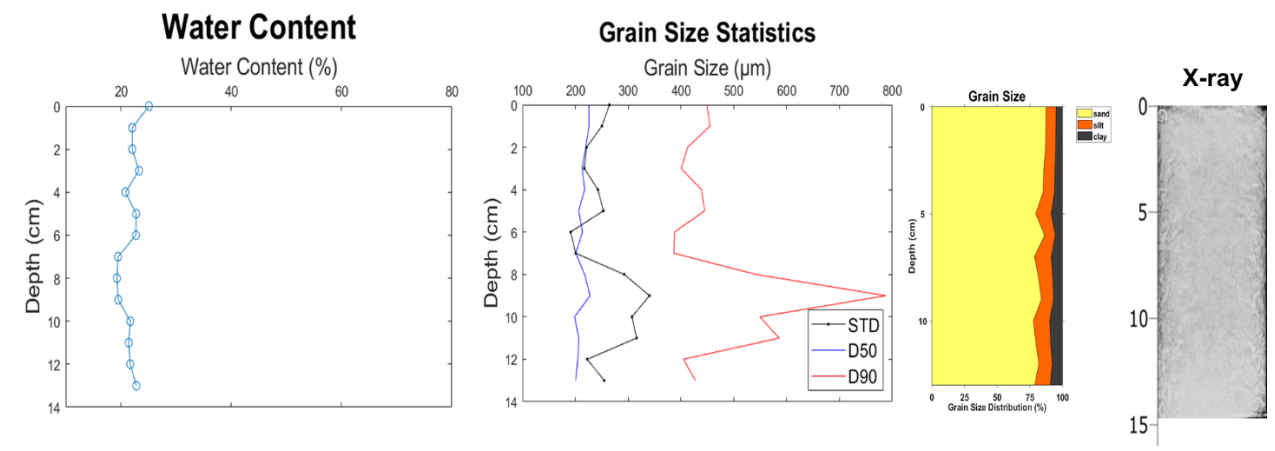

X2-3: July 12, 2018 Data

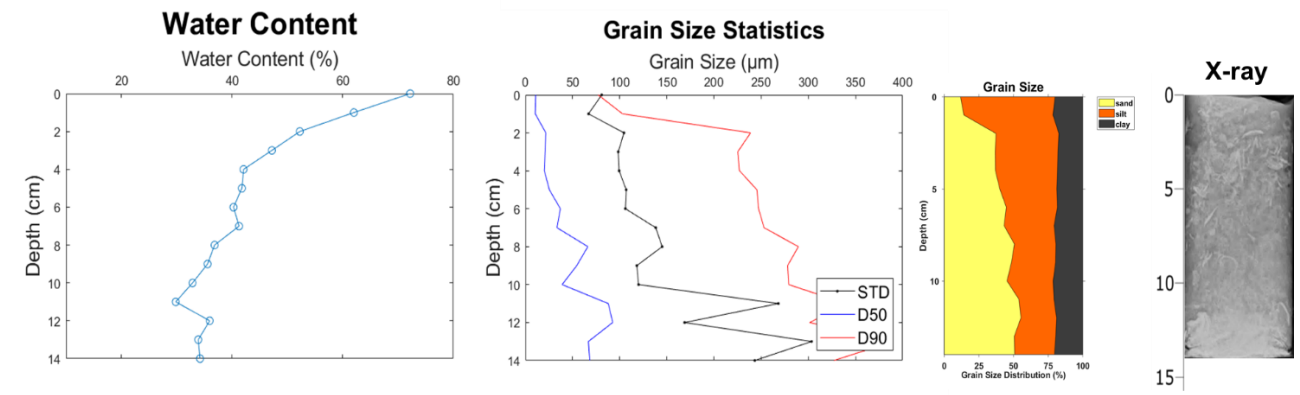

X3-1: July 12, 2018 Data

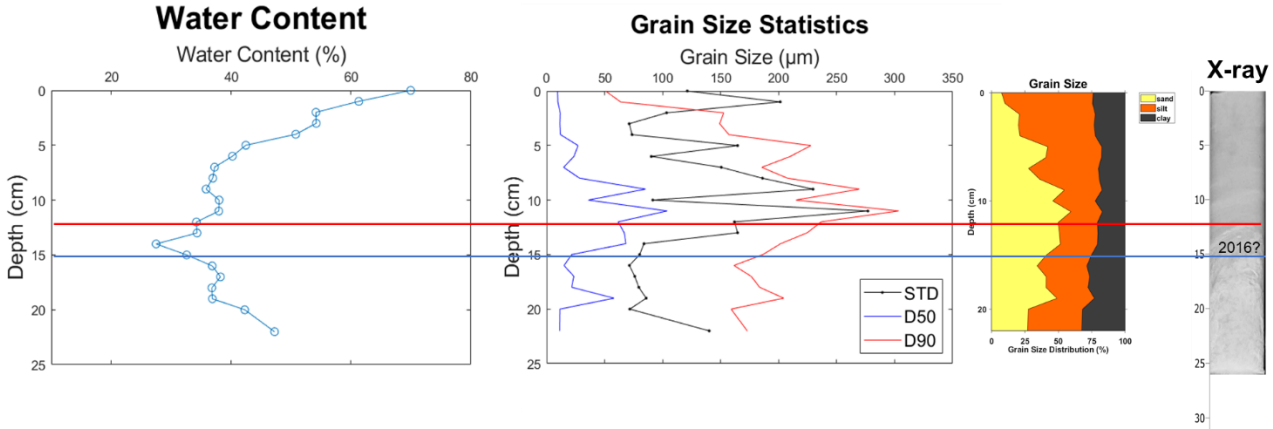

X3-2: July 12, 2018 Data

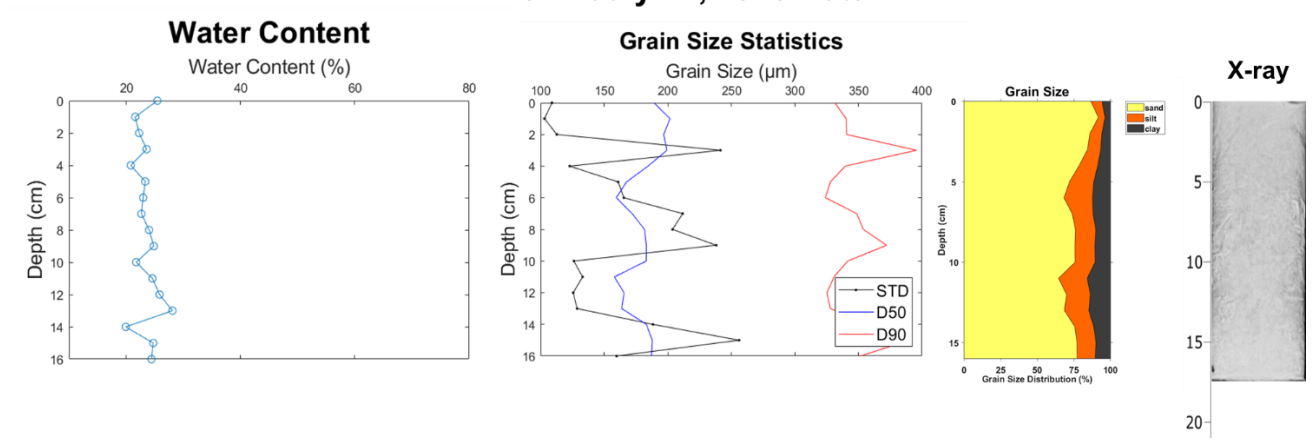

X3-3: July 12, 2018 Data

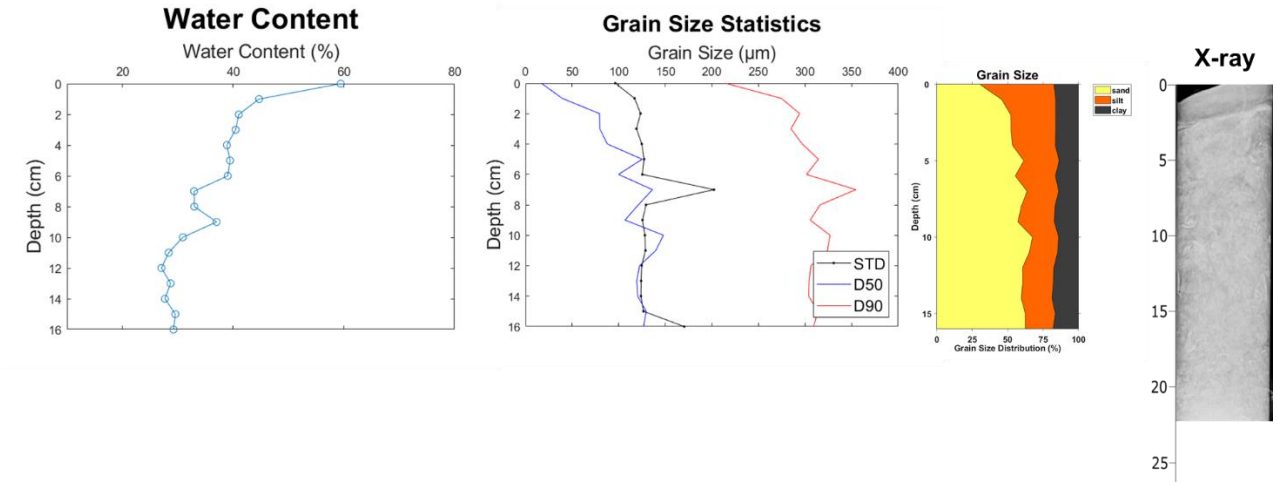

X4-1: July 12, 2018 Data

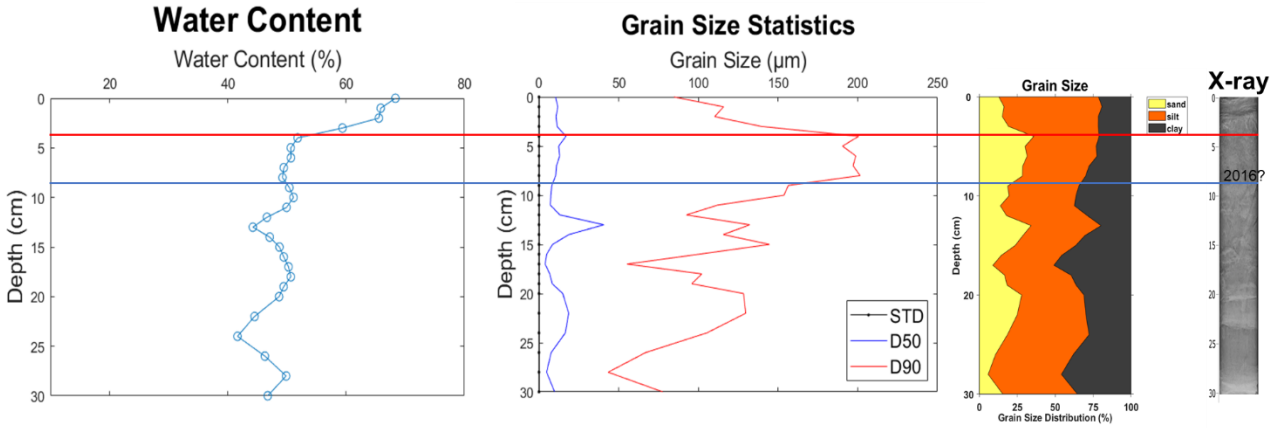

X4-2: July 12, 2018 Data

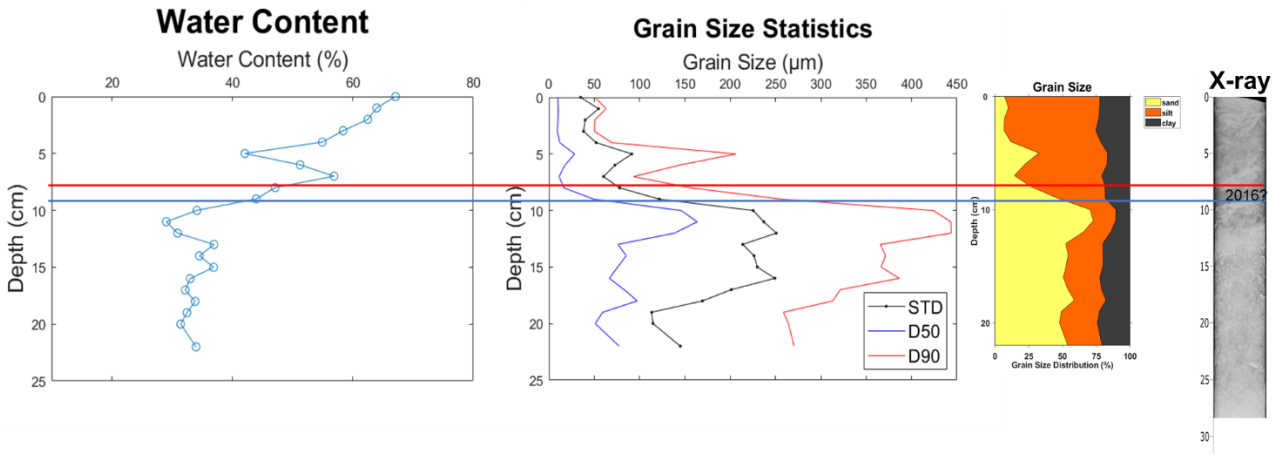

X5-1: July 12, 2018 Data

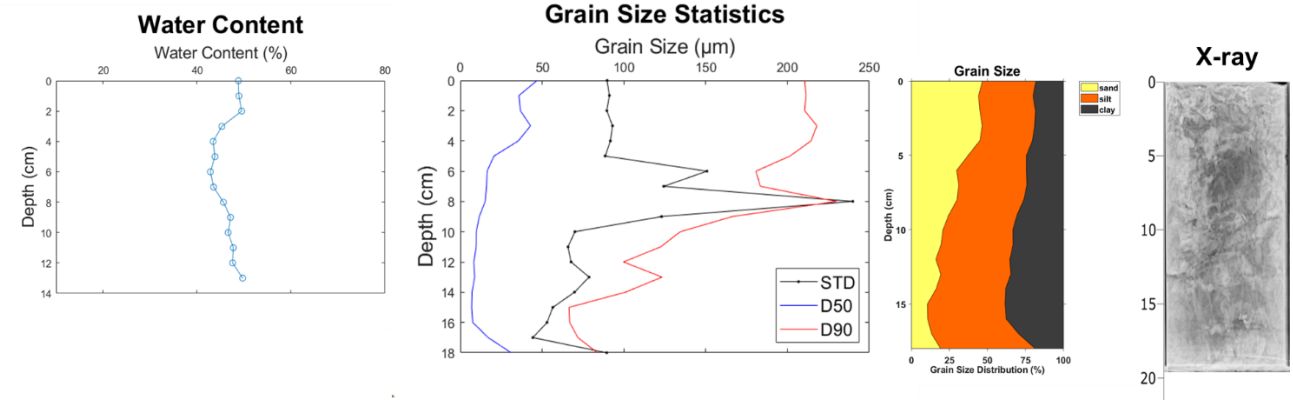

X5-2: July 12, 2018 Data

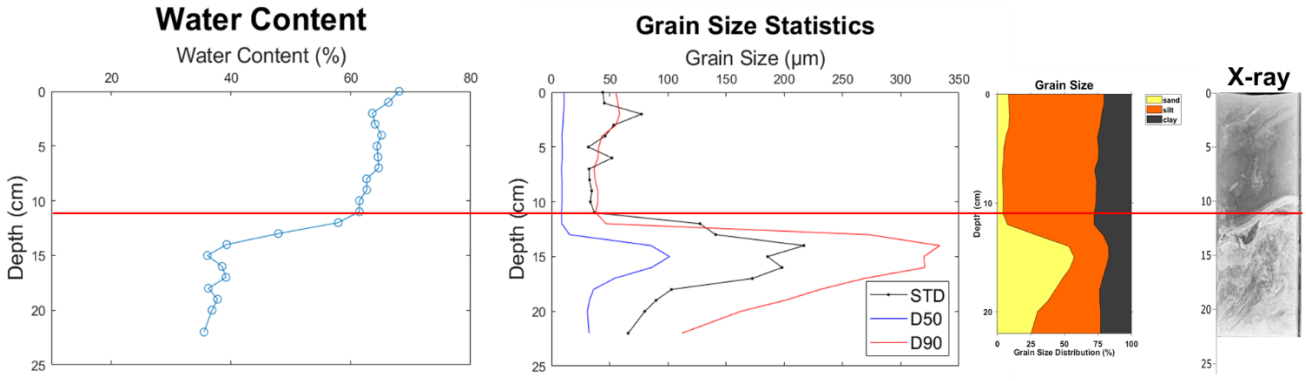

X5-3: July 12, 2018 Data

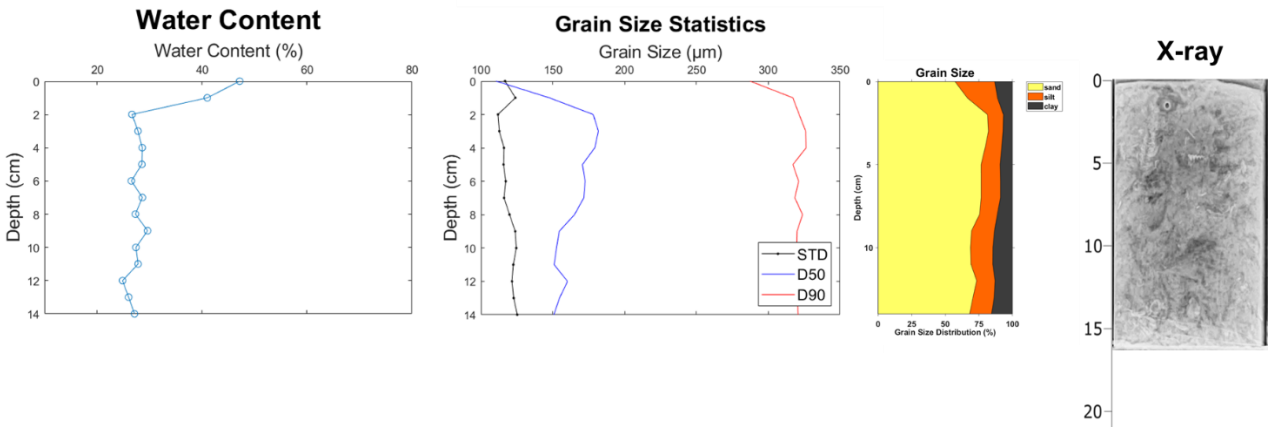

X5-4: July 12, 2018 Data

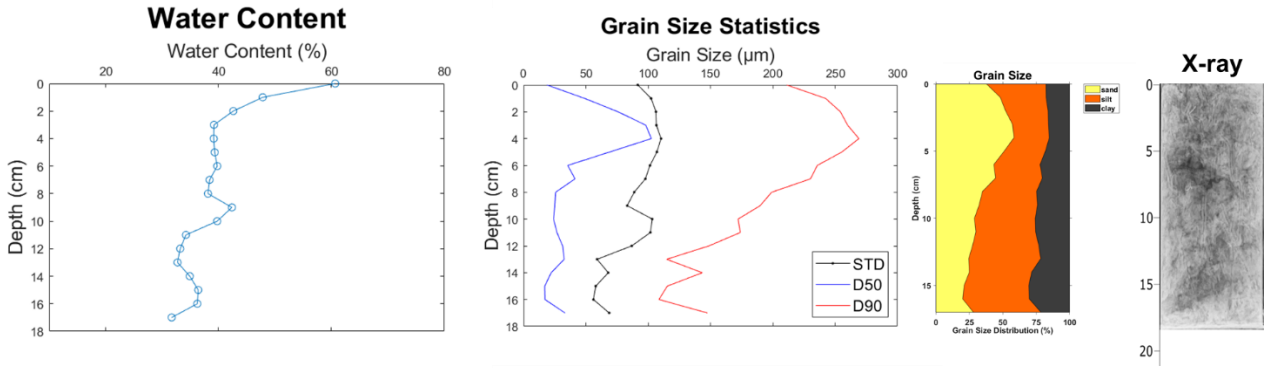

X6-1: July 12, 2018 Data

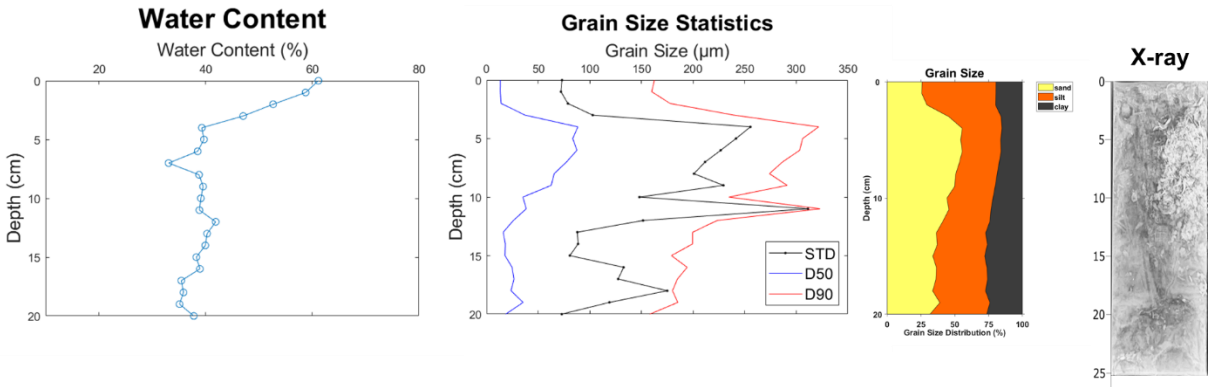

X6-2: July 12, 2018 Data

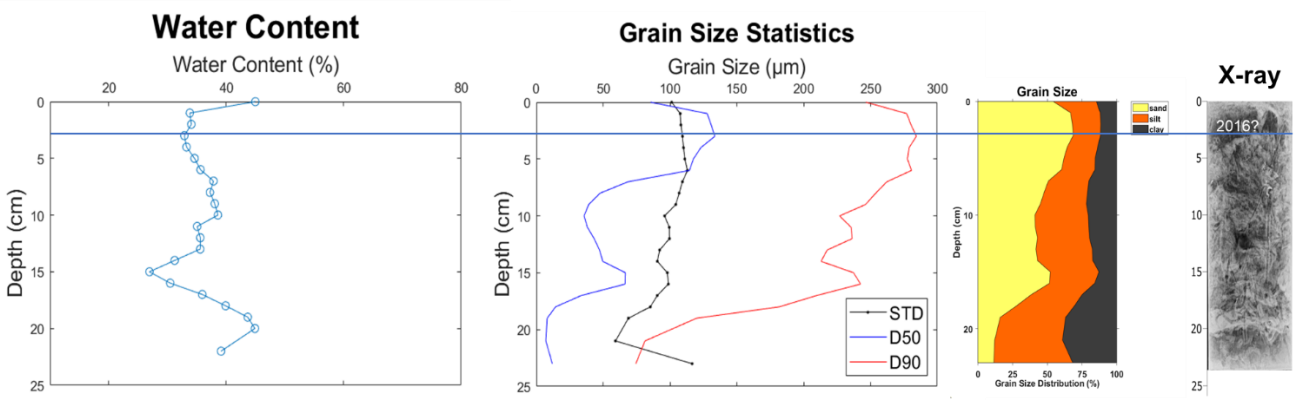

X6-4: July 12, 2018 Data

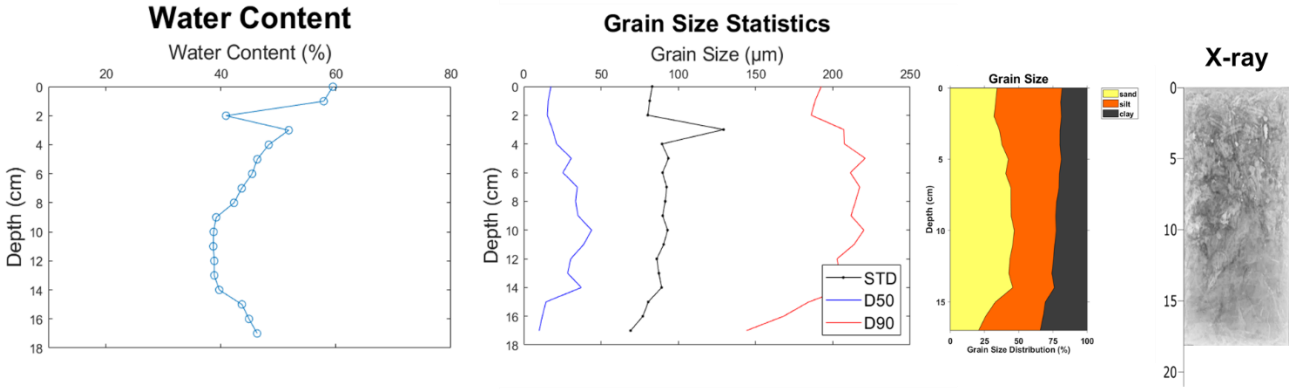

X7-1: July 12, 2018 Data

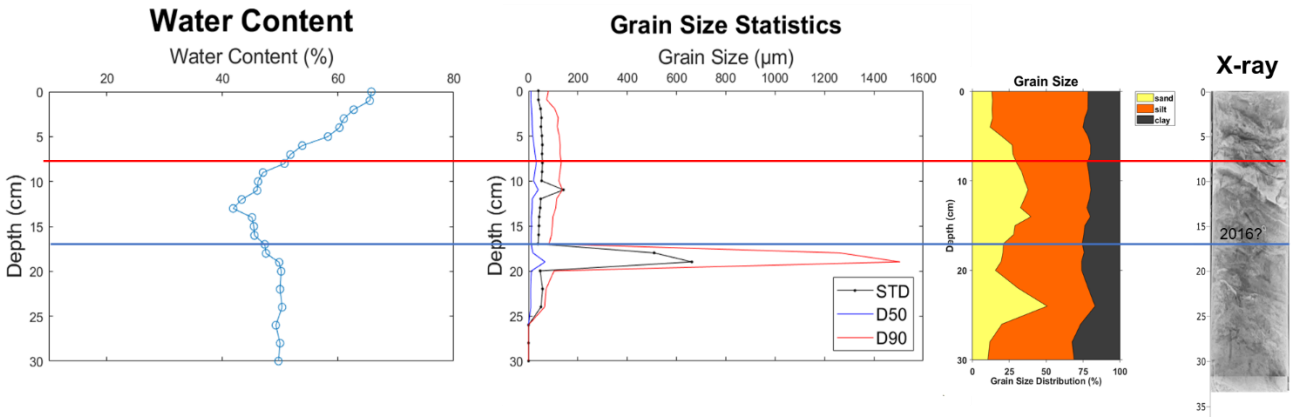

X7-2: July 12, 2018 Data

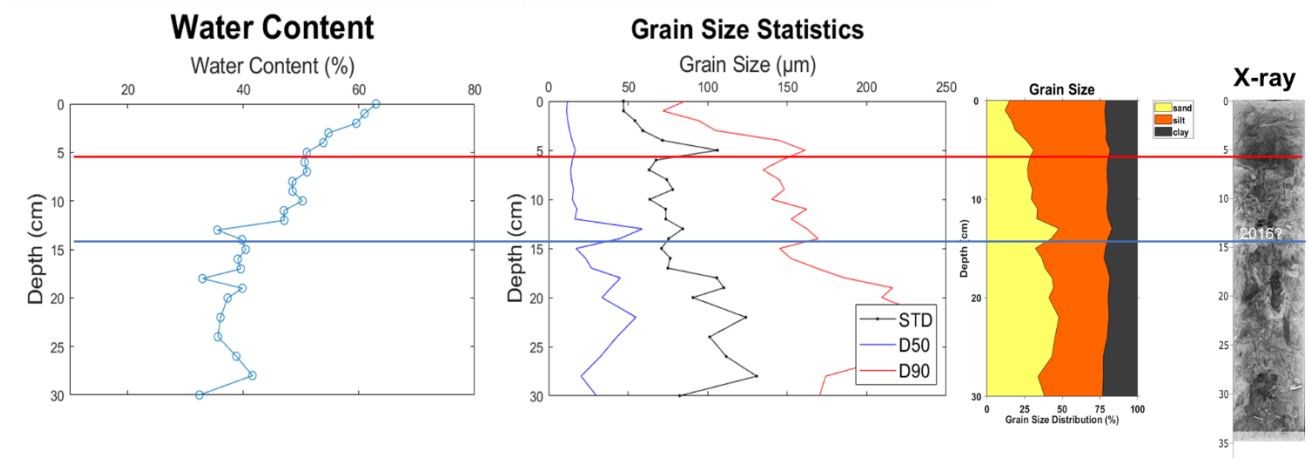

X7-3: July 12, 2018 Data

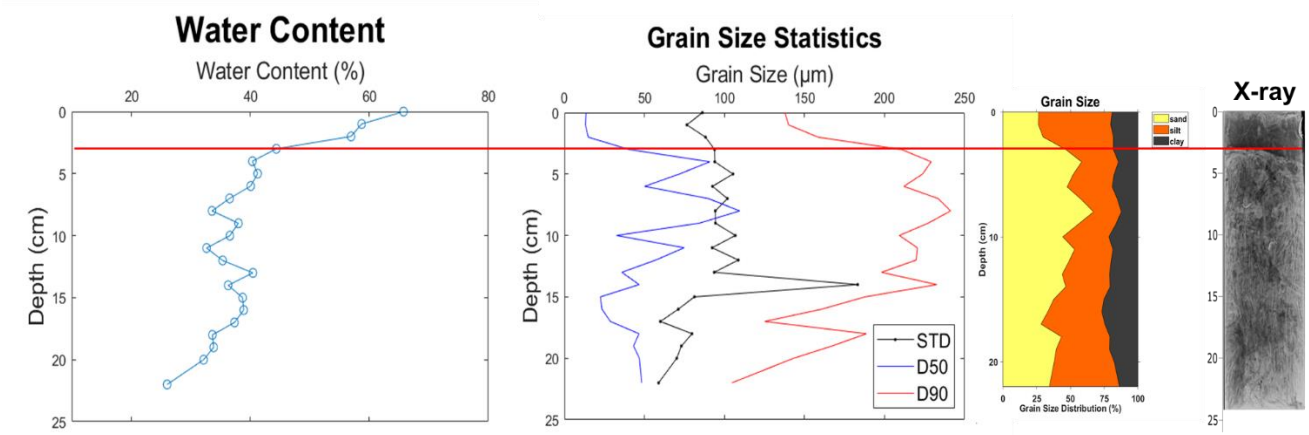

X7-5: July 12, 2018 Data